UNIVERSITÀ
DI PAVIA

DIPARTIMENTO DI SCIENZE DEL FARMACO

Direttore Chiar.ma Prof.ssa Simona Collina

LAUREA MAGISTRALE A CICLO UNICO IN CHIMICA E TECNOLOGIA FARMACEUTICHE

DEVELOPMENT OF CHONDROITIN SULFATE-BASED DISSOLVING MICRONEEDLES AS A PROMISING STRATEGY FOR PROTEIN VACCINE DELIVERY AND IMMUNOMODULATION

Relatore: Prof.ssa Silvia Stefania Rossi

Correlatore: Caterina Valentino

Tesi di Laurea Magistrale a Ciclo Unico di

Alessia Ricotti
Matricola 500795

Anno Accademico 2025/2026

1. INTRODUCTION

2. SKIN

The skin is a large and highly complex organ that performs many essential functions, such as protection, immune defense, and sensory perception. It is organized into three main layers: the epidermis, which is the outer layer, the dermis in the middle, and the hypodermis, the deepest layer as shown in Figure 1

Together with its appendages, the skin forms the integumentary system, which covers the entire body surface and consists of two main components: the skin itself and its appendages (hair, nails and various types of exocrine glands) [1]. At the level of the nostrils, lips, anus and the openings of the urethra and vagina, the skin folds inward and becomes continuous with the mucous membranes lining the respiratory, digestive, urinary and reproductive tracts. In these areas the epithelia connect without interruptions keeping intact the barrier function.

All four fundamental tissues types contributes to skin structure: the skin surface is covered by epithelial tissue; while the underlying connective tissues provides strength and elasticity. Smooth muscle tissue regulates the diameter of blood vessels and the position of hairs present on the body surface, whereas nervous tissue controls both the action of the muscles and the perception of the tactile, pressure, thermal and pain stimuli [2].

The skin acts as the first physical barrier against the external environment, protecting the body from microorganisms, dehydration, ultraviolet radiation, and mechanical injury. It also plays a major sensory role, as the perception of pain, temperature, touch, and pressure originates from specialized receptors located within the tissue. Furthermore, the skin contributes to body movement by allowing smooth and flexible motion.

The skin also performs important endocrine, exocrine and immune functions. Its endocrine role is mainly related to the initiation of biochemical processes

responsible for vitamin D synthesis, which is necessary for calcium absorption and bone metabolism. Its exocrine activity is demonstrated by the release of substances such as water, urea, ammonia, sebum, sweat, and pheromones. At the same time, the skin supports immune defense by secreting bioactive molecules, including cytokines, which help protect the body against pathogens and regulate immune responses.

Another crucial role of the skin is the regulation of body temperature, as it helps maintain thermal balance by either conserving or dissipating heat and also contributes to preserving water balance and overall homeostasis within the body [3]. In this context, skin lipids play a key structural and functional role. These hydrophobic molecules are crucial for maintaining the skin barrier, as they reduce excessive transepidermal water loss (TEWL) and help block the penetration of microorganisms, allergens, and other foreign substances [4].

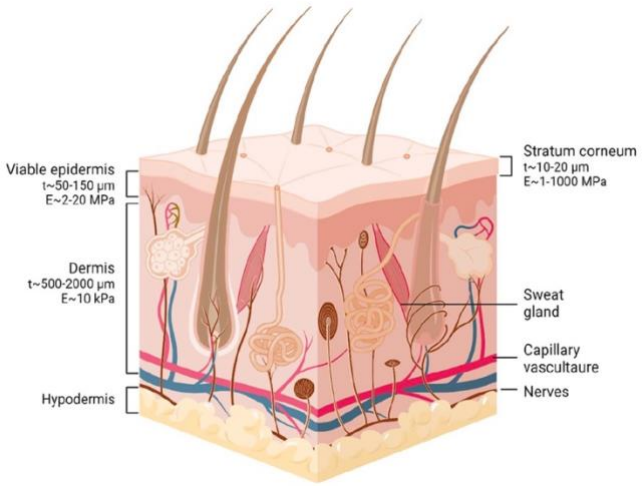

Figure 1: General view of the skin layers [5].

2.1 Epidermis

The epidermis is composed of a stratified squamous keratinized epithelium and represents the outermost layer of the skin. It contains four main types of cells. Keratinocytes are the most abundant cell type and are primarily responsible for the progressive formation of the keratinized barrier. Other less numerous non-epithelial cells are distributed among the keratinocytes in specific epidermal

regions. These include melanocytes, which produce melanin, Merkel cells, which are involved in tactile sensation, and Langerhans cells, which act as antigen-presenting cells in the immune response [1].

From the deepest to the most superficial region the epidermis is divided into the stratum basale, stratum spinosum, stratum granulosum, stratum lucidum, and stratum corneum [6]. The stratum basale is characterized by the presence of basal stem cells, whose division replaces the keratinocytes lost in the superficial layers. Melanocytes are also located in this layer and transfer melanin to the surrounding keratinocytes through their cytoplasmic processes, contributing to skin pigmentation. When a basal stem cell divides, one daughter cell remains in the basal layer, while the other migrates toward the upper epidermal layers and begins to differentiate into a keratinocyte. In the stratum spinosum keratinocytes are arranged in several layers and are connected by desmosomes, which provide strong intercellular adhesion and give the cells their characteristic spine-like appearance [7]. Melanocytes and Langerhans cells may also be found in this layer [2] [7]. The stratum granulosum is composed of one to five layers of flattened, polygonal cells. These cells represent the final stage of differentiation of keratinocytes originating from the upper portion of the stratum spinosum. Although they are close to becoming fully keratinized, they still retain their nuclei and their cytoplasm contains numerous large, coarse, irregularly shaped keratohyalin granules. Another distinguishing feature of these cells is the presence of small membrane-bound lamellar granules that are rich in lipids. These granules release their contents into the spaces between adjacent cells through exocytosis. The secreted lipid material spreads throughout the intercellular spaces, forming the skin's primary epidermal permeability barrier, which plays a crucial role in preventing water loss and protecting the body from the penetration of harmful external substances [1].

The stratum lucidum can be morphologically identified only in thick, hairless skin, such as that found on the palms of the hands and the soles of the feet [6]. This layer contains flattened cells tightly adhered to one another, that lack cytoplasmic organelles, nuclei and are filled with keratin filaments arranged parallel to skin surface [2].

The stratum corneum is the outermost epidermal layer and represents the main barrier to transdermal drug delivery. It consists of flattened, multilayered, anucleate keratinocytes known as corneocytes, embedded in a lipid-rich extracellular matrix. This matrix is mainly composed of ceramides, cholesterol, and free fatty acids (FFAs), which are mainly composed into planar lipid lamellae [6].

Normally, the stratum corneum is relatively dry, which makes the growth of many microorganisms difficult. However, the efficiency of this barrier is also supported by the continuous secretion from sebaceous and sweat glands. Although the stratum corneum is relatively water-resistant, it is not completely impermeable. Corneocytes remain in this layer for approximately two weeks before being shed through desquamation. Therefore, the deeper epithelial layers and underlying tissues are constantly protected by a dynamic barrier composed of terminally differentiated, dead cells [2].

2.2 Dermis

The dermis is an integrated layer of fibrous and amorphous connective tissue located immediately beneath the epidermis and consists of loose connective tissue overlying dense connective tissue containing a dense network of fibers. It contains nerve structures, vascular networks, epidermal appendages, fibroblasts, macrophages, and mast cells. Its main fibrous components are elastic and collagenous connective tissues [8].

The dermis is composed of two main regions: a superficial papillary layer and a deeper reticular layer. The superficial papillary layer consists of loose connective tissue and contributes to the mechanical attachment between the epidermis and the underlying dermal tissue. It also contains capillaries that supply nutrients to the avascular epidermis, as well as peripheral sensory nerve endings involved in skin sensation.

The deeper reticular layer is mainly composed of a twisted fibrous network of dense irregular connective tissue that surrounds blood vessels, hair follicles, nerves, and sweat and sebaceous glands [2]. Owing to its vascularization and innervation, the dermis represents a key target for transdermal and intradermal drug delivery systems, including microneedles.

3. IMMUNOTHERAPY

Autoimmune diseases arise when the immune system loses its ability to distinguish self from non-self, leading to an aberrant attack against the body's own tissues. These disorders represent a heterogeneous group of conditions affecting approximately 3–10% of individuals in the United States and Europe, with considerable variability in clinical presentation, age of onset, and therapeutic response. Their pathogenesis is complex and multifactorial, involving both B lymphocytes, through autoantibody production, and autoreactive T lymphocytes, which contribute to the development of organ specific as well as systemic autoimmune diseases [9].

Conventional therapeutic strategies have historically relied on broad immunosuppression, ranging from glucocorticoids to small-molecule inhibitors and biologic agents. Although these treatments can alleviate symptoms and partially modulate immune dysfunction, they rarely provide a definitive cure and often require long-term administration, exposing patients to complications such as infections and malignancies. The introduction of biologic therapies represented a

major advancement by enabling more selective immunomodulation; however, these approaches still frequently fail to achieve sustained disease remission and may be associated with significant adverse effects over time.

In parallel with the rapid expansion of immunotherapeutic approaches in oncology, interest has been directed toward the application of immunotherapy in autoimmune diseases [10]. Immunotherapy can generally be divided into active and passive strategies. Active immunotherapy aims to stimulate the patient's immune system to recognize and eliminate pathogenic targets while promoting long-term immune memory. Conversely, passive immunotherapy involves the administration of preformed immune components, such as antibodies, cytokines, or immune cells, to provide an immediate therapeutic effect without inducing durable immune memory.

Among these emerging strategies, cellular immunotherapy has gained particular attention as a promising and innovative approach for autoimmune disease management [11]. Rather than simply suppressing immune activity, cellular therapies aim to reprogram or restore immune tolerance at the cellular level. Current approaches under investigation include chimeric antigen receptor (CAR) T-cell therapy, regulatory T-cell therapies designed to promote immune tolerance, and engineered T-cell receptor (TCR) therapies. Many of these strategies involve either the expansion of naturally beneficial immune cell populations or the genetic engineering of patient-derived cells to selectively target pathogenic immune responses through cytotoxic or immunomodulatory mechanisms. Collectively, these therapies hold the potential to provide more precise, durable, and disease-modifying treatments while preserving, and potentially enhancing, the protective functions of the immune system [10].

3.1 Vaccines

Infectious diseases have represented a major challenge throughout human history, and the development of vaccines has profoundly improved global public health. Through widespread vaccination programs, numerous infectious diseases have been eradicated, effectively controlled, or significantly reduced, contributing to increased life expectancy and allowing many generations to survive into adulthood [12]. Vaccination remains one of the most cost-effective and impactful medical interventions ever introduced, substantially reducing morbidity, hospitalization, and mortality associated with infectious diseases [13].

Vaccines function by mimicking natural infections and stimulating the immune system to develop protective immunity without causing the full pathological consequences of the disease. Traditionally, vaccines can be classified into three main categories: whole-pathogen vaccines, subunit vaccines, and nucleic acid vaccines. Whole-pathogen vaccines include both live attenuated vaccines, which use weakened forms of pathogens, and inactivated vaccines, in which pathogens are chemically or thermally neutralized. Subunit vaccines instead rely on purified or synthetically produced pathogen components to induce an immune response, whereas nucleic acid vaccines deliver genetic material, such as plasmid DNA or messenger RNA, encoding specific antigens.

Nevertheless, emerging pathogens continue to expose important limitations in current vaccine and immunotherapy technologies [13]. The COVID-19 pandemic particularly underscored the urgent need for vaccines that can be rapidly developed, easily distributed without complex cold-chain requirements, and capable of inducing potent and durable immune responses. Similar challenges are also evident in cancer immunotherapy, where achieving selective and effective immune responses against poorly immunogenic or poorly detectable tumor antigens remains challenging. Consequently, ongoing research is focused not only on identifying novel vaccine antigens but also on improving delivery systems and

immunotherapeutic strategies to better address rapidly evolving infectious diseases and other complex pathologies [14].

In this context, biomaterials have emerged as promising tools for next-generation vaccines and immunotherapies across infectious diseases, cancer, and autoimmune disorders. These systems include polymeric and lipid nanoparticles, engineered scaffolds, and biodegradable materials, which may be synthetic, naturally derived, or hybrid in composition. A key advantage of biomaterials lies in their high degree of tunability, enabling precise control over antigen loading, cargo protection, release kinetics, and targeting of specific tissues or immune cell populations [15]. By integrating advanced engineering technologies with immunological approaches, biomaterial-based platforms offer the potential to enhance vaccine stability, simplify distribution and storage, and generate stronger, more selective, and longer-lasting immune responses [13].

3.2 Parenteral routes for vaccine administration

Most currently licensed vaccines are administered through parenteral routes, which remain the standard approach for vaccine delivery. Parenteral administration mainly includes three major routes (Figure 2): intramuscular (IM), subcutaneous (SC), and intradermal (ID) injection. These methods are widely used because they allow efficient antigen delivery and the induction of systemic immune responses. Recently developed vaccines against COVID-19, including mRNA-based formulations, are also primarily delivered through parenteral administration.

The route of administration plays a critical role in determining the type, magnitude, and duration of the immune response. Depending on the desired immunological outcome, vaccines may be delivered into the muscle, dermis, or subcutaneous tissue. Each anatomical site contains distinct cellular populations and vascular characteristics that influence antigen uptake and immune activation. In particular, the dermal layer is rich in antigen-presenting cells (APCs), whereas muscular

tissue allows the administration of larger vaccine volumes and and is commonly used for adjuvanted formulations.

Traditional vaccine delivery relies on hypodermic needles; however, increasing attention has been directed toward alternative delivery technologies, including disposable jet injectors and microneedle systems. These approaches aim to improve patient compliance, reduce needle-stick injuries, minimize biohazardous waste, and potentially enhance vaccine stability and immunogenicity. In addition, sustained antigen release, achieved through innovative delivery systems, may further enhance immune priming by prolonging antigen exposure to APCs and promoting stronger adaptive immune responses.

Although parenteral vaccination is highly effective in generating systemic immunity, it generally induces limited mucosal immune responses compared with mucosal vaccination strategies. Moreover, each parenteral route presents specific advantages and limitations in terms of immunogenicity, reactogenicity, ease of administration, and clinical applicability [16,17].

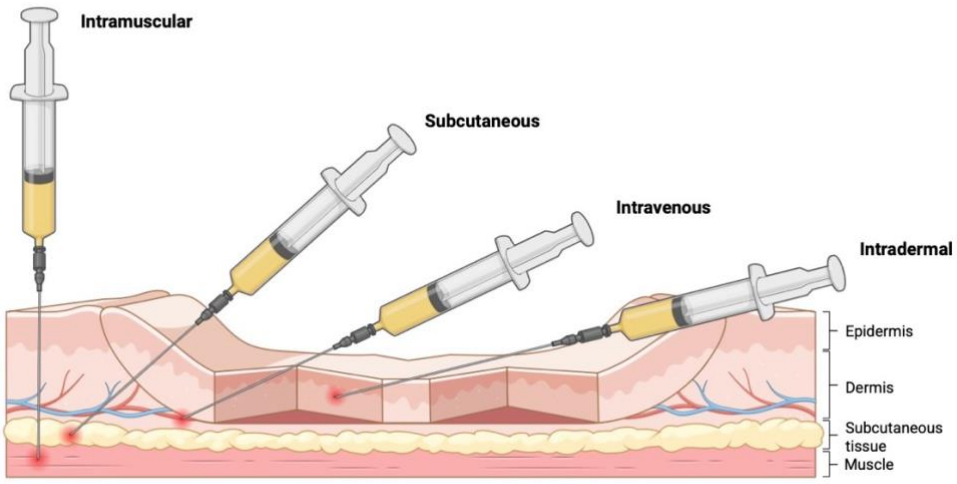

Figure 2: Parenteral routes for administration, BioRender.

3.2.1 Intramuscular injection

Intramuscular vaccination is one of the most commonly used routes for vaccine administration. Vaccines are typically injected into the anterolateral thigh in infants and toddlers up to two years of age, and into the deltoid muscle of the upper arm in older children and adults, in accordance with the Centers for Disease Control and prevention (CDC) recommendations.

Most inactivated vaccines are administered via the IM route because muscular tissue can accommodate relatively large injection volumes and allows gradual antigen absorption. Recently developed mRNA vaccines against COVID-19, such as the Pfizer-BioNTech and Moderna vaccines, are also administered intramuscularly. These vaccines induce strong systemic immune responses, mainly characterized by the production of antigen-specific antibodies and cellular immune activation.

Compared with other parenteral routes, IM vaccination is generally associated with fewer local adverse reactions. Muscle tissue contains fewer pain receptors and lower densities of immune-reactive cells than the dermis or subcutaneous tissue, which may contribute to reduced inflammation and discomfort at the injection site.

The efficacy of intramuscular vaccination can also be influenced by the anatomical site and injection depth. In fact, several studies have demonstrated lower immunogenicity when vaccines are injected into the buttocks compared with the thigh or deltoid muscle. Appropriate needle length is therefore essential to ensure accurate deposition of the vaccine into the muscle tissue. Longer needles have been associated with improved vaccine efficacy and reduced local reactions by allowing deeper and more accurate intramuscular administration.

Despite its advantages, IM administration generally induces limited mucosal immunity, particularly in terms of secretory IgA responses. Nevertheless, it remains the preferred route for many vaccines due to its safety profile, high dose efficiency, and ability to induce robust systemic immune responses [16–18].

3.2.2 Subcutaneous injection

Subcutaneous vaccination involves injection into the tissue layer located between the skin and the muscle. The anatomical site selected for SC administration also influences vaccine performance and tolerability. The CDC recommends the anterolateral thigh for infants and the upper-outer triceps region for individuals older than 12 months of age. Proper injection technique and needle selection are important to ensure accurate placement into the subcutaneous tissue while avoiding unintentional intramuscular or intradermal delivery.

This route is commonly used for the administration of live attenuated vaccines, including the yellow fever vaccine. The subcutaneous tissue allows relatively slow antigen absorption and prolonged antigen exposure, which may support sustained immune stimulation.

In clinical studies, SC administration has generally produced immune responses comparable to those achieved through intramuscular injection, although the magnitude of the response may vary depending on the vaccine formulation and the presence of adjuvants. Compared with intramuscular administration, SC vaccination is often associated with a higher frequency of local adverse reactions. These may include pain, swelling, induration, nodules, inflammation, and skin irritation at the injection site. Some studies have reported greater discomfort following SC injection compared with IM administration, particularly in pediatric populations receiving vaccines such as *Haemophilus influenzae* type b (Hib) vaccine.

Although SC administration remains widely used for several live vaccines, its higher reactogenicity and lower tolerability compared with IM injection have contributed to the preference for intramuscular delivery for many modern vaccine formulations, particularly those containing adjuvants [16,17].

3.2.3 Intradermal injection

Intradermal vaccination involves the administration of vaccines into the dermal layer of the skin. This route is commonly used for Bacille Calmette-Guérin (BCG) vaccination against tuberculosis and for rabies immunization. The skin is highly immunologically active because it contains large numbers of APCs, including dermal dendritic cells and epidermal Langerhans cells.

Due to the high concentration of APCs, intradermal vaccination can induce stronger immune responses than intramuscular or subcutaneous administration, even when lower antigen doses are used. Antigen capture within the skin promotes dendritic cell maturation and migration to draining lymph nodes, enhancing adaptive immune activation and enabling dose-sparing strategies. For this reason, ID vaccination has been explored in populations with reduced responsiveness to conventional IM vaccination, such as patients undergoing dialysis receiving hepatitis B vaccination.

Despite its immunological advantages, ID administration presents technical challenges. Accurate placement of the vaccine into the dermal layer requires specific expertise and can be difficult using conventional syringes. To overcome these limitations, specialized intradermal delivery devices and microneedle (MN) systems are currently being developed, Figure 3. MN-based vaccine delivery represents a promising innovation in intradermal immunization. These micron-sized patches enable precise delivery into superficial skin layers while minimizing pain and discomfort. Because MNs penetrate only shallowly into the skin, they avoid contact with deeper innervated tissues, reducing needle-associated pain and patient needle phobia. Additionally, MNs may simplify vaccine distribution and potentially reduce dependence on cold-chain storage systems.

However, ID administration is generally associated with more pronounced local adverse reactions compared with IM injection. Common reactions include erythema, itching, superficial skin lesions, nodules, and local inflammation.

Several studies have shown that ID vaccination may produce stronger local reactogenicity than both SC and IM administration, although systemic adverse events are generally comparable [16,17,19].

3.2.4 Microneedles as a new generation vaccine

MNs technology has rapidly emerged as a versatile and promising platform for transdermal drug delivery, demonstrating broad applicability for the administration of nucleic acids, small molecules, proteins, nanoparticles, and other therapeutic agents. In particular, MN-based systems, have attracted significant attention in the field of immunotherapy and vaccination, where they have shown the ability to markedly enhance immune responses in preclinical studies involving influenza vaccines, hepatitis B plasmid DNA, and Bacillus anthracis antigens. Since vaccines remain among the most effective and cost-efficient medical interventions for disease prevention and control, the development of innovative delivery systems capable of improving vaccine efficacy and accessibility is of considerable interest [19]. The skin itself represents an ideal target for immunomodulation because it is a highly immunologically active organ containing numerous immune cell populations, including keratinocytes, macrophages, T cells, Langerhans cells, and dendritic cells. In particular, Langerhans cells and dendritic cells, act as professional antigen-presenting cells capable of capturing antigens and activating adaptive immune responses. Consequently, transcutaneous immunization (TCI) has often been shown to induce stronger immune responses than traditional intramuscular or subcutaneous injections while potentially requiring lower antigen doses. Despite these advantages, the outermost layer of the skin, the stratum corneum, represents a major barrier to the delivery of macromolecules and antigens [20]. MN technology was introduced to overcome this limitation by creating microscale channels that allow therapeutic agents to

penetrate the epidermis and upper dermis, where immune-cell populations are highly concentrated. Compared with standard subcutaneous injections, MN-based immunotherapy offers several important advantages, including painless administration, reduced invasiveness, improved patient compliance, and the possibility of self-application without specialized equipment. In addition, MNs can incorporate therapeutic agents in dry formulations, thereby improving thermal stability and simplifying storage and transportation requirements. These characteristics are especially advantageous for large-scale vaccination campaigns and resource-limited settings [19]. Clinical and preclinical studies have demonstrated that MN-based vaccines can generate immune responses comparable or even superior to those induced by traditional injection-based immunization. As a result, numerous MN-based vaccines are currently under development for infectious diseases such as influenza, measles-rubella, rabies, Ebola, polio, HIV, and SARS-CoV-2 [20].

4. MICRONEEDLES

After their introduction as innovative skin-based delivery systems, MNs have progressively evolved into versatile platforms for drug delivery, vaccination, diagnostics, and cosmetic applications. Their development results from the convergence of transdermal delivery, microfabrication, materials science, and biomedical engineering. This chapter describes the historical evolution of microneedle technology, followed by its main structural characteristics, classification, fabrication materials, and mechanisms of action.

4.1 History of microneedles

Over the years, the concept of MNs has progressively evolved from early skin perforation techniques to the advanced MNs devices used for drug delivery, vaccination, diagnostic, and cosmetic applications.

In 1905, the German dermatologist Ernst Kromayer treated scars, hyperpigmentation, and various skin conditions using motorized dental burs of different sizes. Although this approach was not a MNs system in the modern sense, it represented an early example of controlled skin perforation for therapeutic purposes.

The earliest documented use of the term “microneedles” appeared in 1921, when Chambers described the insertion of a fine needle into the nucleus of an egg without causing apparent injury. During the 1960s, interest grew in drug delivery strategies through injections into the stratum corneum. Later, in the 1970s, the idea of using MNs for transdermal drug delivery was formally proposed, although practical experimental demonstrations emerged later, in the 1990s, mainly with the development of microfabrication techniques.

A major milestone in transdermal delivery occurred in 1979, when the first system transdermal therapeutic system, a three-day scopolamine-releasing patch for the treatment of motion sickness, was approved. Despite this device did not contain MNs, it contributed to establishing transdermal administration as a clinically relevant drug delivery route. In 1994, Orentreich introduced subcision surgery, using a tri-beveled hypodermic needle inserted beneath the skin to break fibrous tissue strands associated with wrinkles and depressed scars. This procedure further highlighted the therapeutic potential of controlled mechanical intervention within the skin.

The first MN specifically designed for transdermal drug delivery was proposed in 1998. It was produced from silicon wafers using microfabrication techniques such

as ion etching and photolithography techniques, demonstrating that microstructured needles could enhance drug transport across the skin. This work sparked extensive research into MN-based delivery systems and encouraged the exploration of different materials, including glass, ceramics, metals, and polymers, for microneedle fabrication [20].

In 2004, MN arrays were used to create microscopic openings in the skin for transdermal drug delivery, encouraging the development of multiple fabrication approaches and materials for transdermal drug delivery (TDD) applications. Different types of MNs were subsequently developed, including solid, coated, hollow, dissolving, and hydrogel-forming types. In parallel, manufacturing techniques such as laser ablation, photolithography, and micro-injection molding gained importance. These advances led to the development of dissolving MNs for transdermal drug delivery, further expanding the potential of MN technology toward safer, more patient-friendly, and more versatile delivery platforms [21].

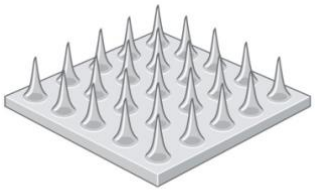

Figure 3: MN patch, BioRender

4.2 Microneedle's general features

MN technology represents an active transdermal drug delivery approach designed as an alternative to conventional syringe-based injections as shown in Figure 4. MN arrays penetrate the stratum corneum and deliver drugs through a minimally invasive mechanism. These arrays consist of microscopic needles typically ranging from 25 to 2000 μm in height [22]. MNs have been widely applied in areas such as drug and vaccine administration, cosmetics, and disease diagnostics. They can

be different in structure, geometry, material composition, and fabrication techniques.

The effectiveness of MN-based drug delivery can be influenced by several external factors, including skin physiology, physicochemical characteristics, and surrounding environmental conditions. Parameters such as temperature and relative humidity near the application site play an important role. Low humidity levels can slow drug release into the skin layers, whereas excessive humidity, including perspiration, may alter drug release kinetics because of additional moisture and dissolved salts that affect osmotic gradients during transdermal delivery. Heavy sweating may also reduce patch adhesion to the skin, thereby limiting efficient drug permeation. In addition, extremely acidic or alkaline pH conditions around the skin surface can decrease drug permeability through the stratum corneum. Lipid-rich films on the skin can create an additional barrier to absorption, while removing these lipids may improve transdermal uptake. Increasing skin temperature can further promote drug permeation due to enhanced molecular diffusion and vasodilation of blood vessels in the skin [20]. An important consideration in MNs systems is the precision of drug loading and dosage control, especially for medications such as insulin or chemotherapeutic agents. Compared with oral administration, MN patches generally require smaller doses to achieve similar therapeutic effects because they bypass digestion and first-pass metabolism. The pharmacokinetic profile of MNs allows rapid absorption into the bloodstream, which is particularly useful for localized treatments while requiring lower drug quantities than oral delivery methods [23]. The amount of drug incorporated into a MNs system depends on factors such as the drug itself, the intended treatment strategy, and patient-specific requirements. MNs provide highly accurate drug delivery because of the controlled manufacturing and loading processes involved. Nevertheless, drug dissolution and release at the skin interface can still be affected by skin characteristics, environmental conditions, and the way

the device is applied to the skin surface. MNs are considered one of the most effective approaches for transdermal drug delivery because medications administered through this method bypass major organs such as the liver. In addition, MNs avoid the pain commonly associated with intravenous injections, offering a nearly painless administration process. For this reason, they are particularly suitable for individuals affected by needle phobia, also known as trypanophobia. Another advantage of MN-based drug delivery is that it does not require highly trained medical staff, making the system easier and more convenient to use. Moreover, the technique lowers the risk of infection transmission during drug administration [24]. The stratum corneum functions as a protective barrier that prevents therapeutic molecules from penetrating the skin and reaching the epidermal or dermal layers. MNs are capable of overcoming this barrier by creating microscopic pathways that allow drugs to be delivered directly into the epidermis or upper dermis without causing pain. In addition, MN arrays are specifically designed to be long enough to cross the stratum corneum while remaining short enough to avoid damaging deeper dermal tissues or stimulating nerve endings, which contributes to their painless application [25].

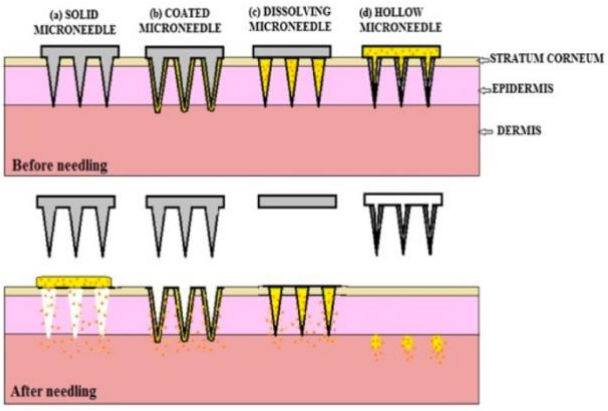

Figure 4: Types of Mns [20].

4.3 Application

MNs have emerged as a versatile platform in the biomedical field, offering minimally invasive solutions for drug delivery, diagnostics, and therapeutic applications. Their microscale dimensions allow them to penetrate the skin barrier without stimulating pain receptors, thereby improving patient compliance and enabling efficient access to underlying tissues [26,27]. One of the most established applications of MNs is transdermal drug delivery. In this context, MNs facilitate the administration of therapeutic agents into systemic circulation, overcoming the limitations associated with oral administration and conventional injections. These systems can be integrated with wearable electronics, allowing personalized and dynamic healthcare monitoring and supporting the development of point-of-care diagnostic devices [28]. Furthermore, MNs are increasingly combined with nanomedicine approaches, particularly nanoparticles, to enhance drug delivery performance by protecting active compounds from degradation, enabling sustained release, and facilitating targeted delivery to specific tissues. This combination overcomes the limitations of conventional transdermal systems by improving penetration through the skin barrier. Finally, emerging applications of MNs include targeted drug delivery to tumors and other specific tissues, as well as delivery to organs beyond the skin, such as the eye, oral mucosa, and gastrointestinal tract, often within advanced systems that integrate sensing and therapeutic functions in theranostic programme [26,28] . Overall, MNs represent a highly promising technology with broad applications across multiple medical fields, and their continued development is expected to significantly impact the future of personalized and precision medicine.

4.4 Geometry

The geometry of MNs plays a fundamental role in determining their mechanical performance, skin penetration capability, and overall effectiveness in biomedical

applications. MNs are typically characterized by dimensions in the micrometer range, with heights of several hundred micrometers and tip diameters ranging from a few to several tens of micrometers, and they are often arranged in arrays to enhance their functional performance. The morphological and geometrical design of MNs is widely recognized as a critical factor influencing their ability to penetrate the skin, deliver drugs, and extract interstitial fluid, as well as their clinical outcomes [29]. In particular, parameters such as shape, height, base diameter, tip geometry, and spacing between needles collectively determine both the mechanical strength of the MNs and the forces required for insertion into the skin, Figure 5. Among the various geometric configurations, conical and pyramidal shapes are the most commonly used due to their compatibility with fabrication techniques such as micro-molding, although more complex geometries have been developed to improve performance [30]. For example, certain geometries reduce the force required for insertion or increase the contact surface area, thereby improving drug loading and release profiles [29]. Additionally, the number of faces in pyramidal MNs can influence insertion efficiency, with multi-faceted designs showing improved penetration compared to simpler geometries [30].

4.5 Diameter

The geometry of the MN tip is particularly crucial, as it directly affects the penetration force required to breach the stratum corneum. Sharper tips with smaller diameters require lower insertion forces, while blunt tips significantly increase the force needed for skin penetration. However, extremely small tip dimensions are not always optimal, as they may compromise mechanical strength or reduce drug-loading capacity, highlighting the need for a balance between sharpness and robustness [29]. The insertion process itself is governed by multiple forces, including stiffness, bending, buckling, cutting, and friction forces, all of which are influenced by the geometry and dimensions of the MN. A successful design must

therefore ensure that the insertion force exceeds the resistance of the skin while remaining below the fracture threshold of the MN to prevent structural failure [30,31].

4.6 Length

Another key geometric parameter is the height of the MNs, which must be sufficient to penetrate the epidermis without reaching deeper layers containing nerves and blood vessels. Typically, MN heights range from approximately 150 to 2000 μm, with most designs concentrated between 600 and 800 μm to achieve optimal penetration without causing pain or bleeding [5]. The effective penetration depth, however, is usually only a fraction of the total needle length, often between 30% and 60%, due to skin deformation during insertion. The base diameter and aspect ratio (height-to-width ratio) also significantly influence mechanical stability, as wider bases increase stiffness and reduce the likelihood of bending or fracture under applied forces. In general, lower aspect ratios correspond to higher mechanical strength, whereas higher ratios may improve penetration but at the cost of structural integrity [29].

4.7 Density and distance

The arrangement of MNs within an array, including spacing and density, is another essential geometric consideration, Figure 5. Closely spaced needles can increase drug loading and contact area with the skin but may also lead to reduced penetration efficiency due to the so-called “nail bed effect,” where skin deformation prevents all needles from fully penetrating. Conversely, increasing the spacing between needles can reduce the required penetration force and improve insertion efficiency, although it may decrease the total delivered dose. Therefore, an optimal design requires a careful balance between spacing, density, and mechanical performance. Overall, the geometry of MNs is a key determinant of

their functionality, and the optimization of geometric parameters is essential to achieving effective, safe, and reliable performance in drug delivery and diagnostic applications [29,32].

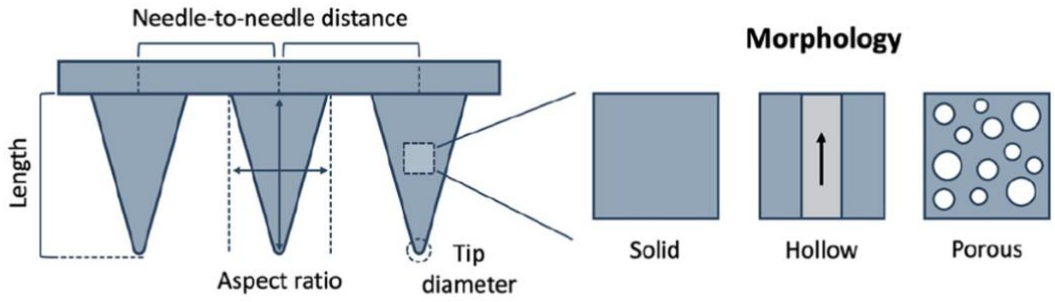

Figure 5: MNs density and distance [5]

4.8 TYPE OF MICRONEEDLES

Various materials, including silicon, stainless steel, sugars, and polymers, have been utilized in the fabrication of different MN designs such as solid, coated, hollow, and dissolving MNs. Each MN category possesses distinct properties, benefits, limitations, applications, and material compositions that influence its performance and suitability for specific biomedical purposes [20].

4.8.1 Solid MNs

Solid MNs are specifically designed to penetrate the stratum corneum and enhance drug delivery into the dermal layer, thereby improving bioavailability and transdermal transport across the skin. In comparison with conventional intramuscular administration, they are particularly effective for vaccine delivery because they can induce longer-lasting effects and stronger antibody-mediated immune responses. In addition, solid MNs are relatively easy to manufacture and generally provide superior mechanical strength and sharper tips than hollow MNs. They can also be fabricated from a variety of materials, including silicon, metals, and polymers, depending on the intended biomedical application. Besides direct

drug administration, MNs may also be employed as a pretreatment strategy for creating micropores in the skin. By penetrating or gently disrupting the skin surface, sharp MNs generate microchannels that facilitate drug transport either for localized therapeutic effects or for systemic delivery through absorption into skin capillaries as shown in Figure 6. After pore formation, drugs can be applied onto the treated area using drug-loaded transdermal patches, similarly to conventional transdermal systems, or through semi-solid topical formulations such as creams, gels and lotions commonly used in dermatological therapies [20,23,33].

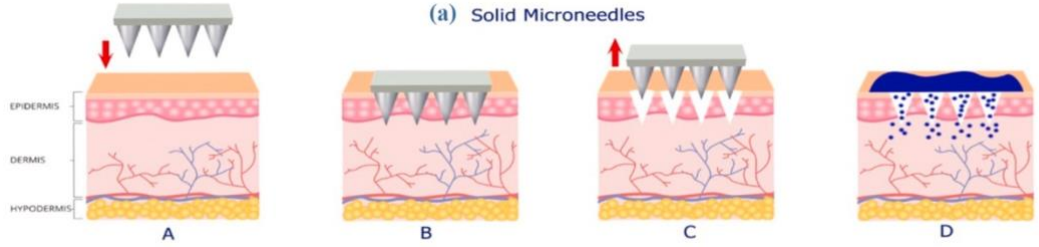

Figure 6: Solid MNs application [34] .

4.8.2 Hollow MNs

Hollow MNs are characterized by the presence of an internal lumen or bore, typically ranging from 5 to 70 μm in diameter, which enables the transport and delivery of liquid drug formulations. Unlike solid microneedles, hollow MNs can administer significantly larger amounts of active pharmaceutical ingredients directly into the viable epidermis or dermis, making them particularly suitable for vaccines, insulin, and other high–molecular weight therapeutics. Drug delivery may occur through passive diffusion or by applying external pressure using systems such as syringes, pumps, gas-driven devices, or integrated microfluidic components. In this “poke-and-flow” approach, liquid formulations generally flow from a connected reservoir through the hollow needles at controlled rates, allowing continuous release into specific skin layers as shown in Figure 7. One of the major advantages of hollow MNs is their ability to precisely regulate drug administration

and release kinetics. Depending on the formulation, device geometry, and fabrication parameters, these systems can achieve either rapid burst release or sustained delivery over extended periods. Compared with other microneedle types, hollow MNs provide higher drug-loading capacity, relatively low manufacturing costs, and accurate control overdosing. Moreover, unlike solid MNs, where drug release is mainly driven by osmotic gradients, hollow systems function as active delivery devices by creating microchannels through which liquid formulations diffuse directly into the dermal tissue. Their geometry, including parameters such as aspect ratio and needle opening configuration, can also be optimized to modulate injection pressure, infusion speed, and time-dependent release behavior. Despite these advantages, hollow MNs present several technical challenges. Their mechanical strength is generally lower than that of solid MNs, requiring careful optimization of insertion techniques and needle design. In addition, clogging of the needle tip and resistance to liquid flow caused by compressed skin tissue may occur during administration. To overcome these limitations, strategies such as side-opened or off-centered needle designs have been developed to improve fluid transport and reduce obstruction during drug delivery [20,21,23].

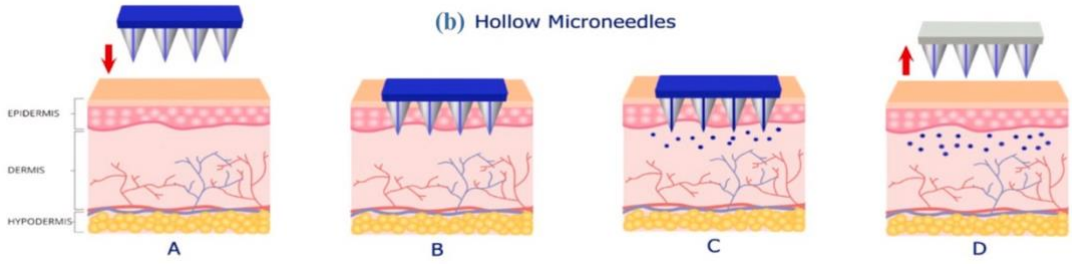

Figure 7: Hollow MNs application [34].

4.8.3 Coated MNs

Coated MNs represent a modified form of solid MNs in which the needle surface is covered with a thin layer containing the active drug formulation. Typically, the

amount of drug delivered depends on the thickness and uniformity of the applied coating, meaning that coated MNs generally administer relatively small doses of therapeutic compounds. For this reason, the efficiency of the system strongly relies on the ability to achieve a precise, homogeneous, and reproducible coating process on the MN surface. These MNs are particularly suitable for the minimally invasive delivery of biomolecules such as proteins, peptides, vaccines, and DNA. A coated MN usually consists of a sharp solid-core structure coated with a solid film composed of the active pharmaceutical ingredient and water-soluble excipients. Besides facilitating the coating process itself, these excipients promote rapid detachment and dissolution of the drug layer once the MNs penetrate the skin. After insertion, the coating comes into contact with the interstitial fluid present within the tissue. This aqueous environment dissolves the water-soluble excipients, triggering separation of the drug-containing film from the MN surface as shown in Figure 8. Depending on the composition and solubility of the coating materials, detachment may occur within seconds or minutes, allowing rapid release of the therapeutic payload before the MNs are removed from the skin. Complete dissolution of the deposited material can then continue gradually within the tissue. One of the main advantages of coated MNs is their ability to provide fast drug release while maintaining a minimally invasive administration route. In addition, studies have demonstrated that vaccine delivery through coated MNs can induce immune responses comparable to those achieved with conventional intradermal or intramuscular injections. Furthermore, coated MNs may also be used for drug delivery to tissues other than skin. However, one potential limitation is the possibility that residual coating material remains attached to the needle tip after administration, which could increase the risk of contamination or infection if the device is reused or improperly handled [20,35,36].

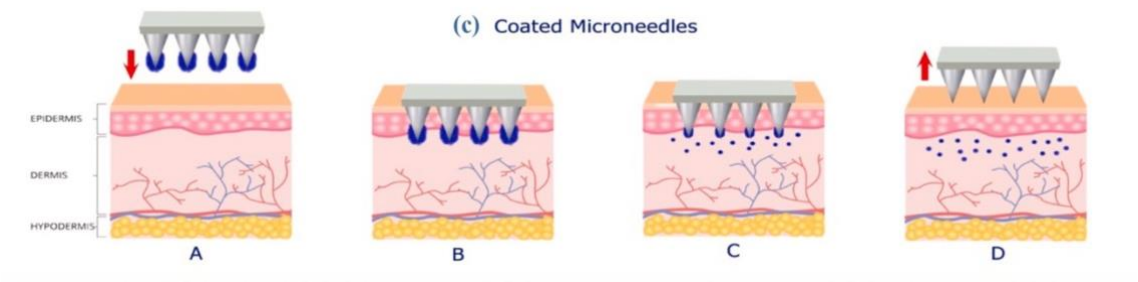

Figure 8: Coated MNs application [34].

4.8.4 Hydrogel-forming MNs

An ideal drug delivery system should be capable of encapsulating active compounds within a biocompatible and mechanically stable structure while ensuring controlled drug release and easy administration with minimal medical supervision. In this context, hydrogels represent a highly promising solution due to their ability to form three-dimensional polymeric networks with high water content, excellent biocompatibility, flexibility, and hemocompatibility. The physicochemical properties of these materials depend on factors such as composition, concentration, crosslinking strategy, and fabrication method, whereas their mechanical characteristics can be precisely tailored through physical or chemical crosslinking [37]. The integration of hydrogels into MN structures has attracted significant attention in biomedical research because it combines efficient drug delivery with a minimally invasive administration approach. Hydrogel-based MNs are generally fabricated as rigid and solid structures with sufficient mechanical strength to penetrate the skin. Once inserted, interstitial fluid diffuses into the polymeric matrix, causing hydration and swelling of the system, which transforms into a hydrogel capable of absorbing large amounts of fluid as shown in Figure 9. This process creates continuous channels through which the active pharmaceutical ingredient can diffuse into the surrounding tissues, enabling controlled drug release. In some cases, the system may subsequently dissolve depending on the internal structure of the matrix [38]. Hydrogel-forming microneedles (HFMs) differ from conventional microneedles because they are

composed of crosslinked polymeric matrices that rapidly swell upon contact with skin fluids, creating a continuous and unobstructed pathway for drug transport. These systems offer several advantages, including high drug-loading capacity, controllable release profiles, and excellent biocompatibility, while also reducing the risk of skin damage associated with needle fracture. More advanced systems, known as extensible and swellable HFMNs, exploit the dynamic deformation properties of polymer chains to extend and swell after insertion into the skin, thereby establishing a continuous connection between the drug reservoir and the dermal microcirculation. Owing to the hydrophilic nature of the hydrogel polymers, these devices promote deeper interaction with local tissues and further enhance therapeutic delivery efficiency [37,39].

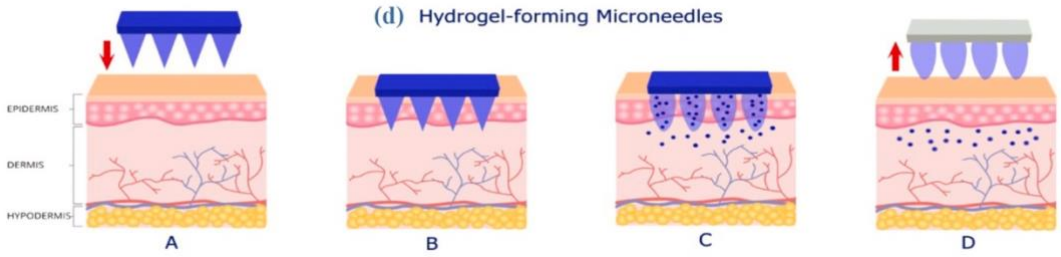

Figure 9: Hydrogel-forming MNs [34]

4.8.5 Dissolving MNs

Dissolving microneedles (DMNs), first introduced in 2005, are an increasingly promising approach for transdermal drug delivery due to their distinctive advantages. One of their main features is the rapid release of macromolecules combined with a simple single-step administration process, which improves ease of use and patient compliance. Because of their “poke-and-release” mechanism, DMNs are often considered superior to several other MN types in specific applications. These systems are typically fabricated by encapsulating the drug within biodegradable or water-soluble polymer matrices using techniques such as

two-step casting or micro-molding. After insertion into the skin, the MN structure dissolves upon contact with interstitial fluid, leading to the controlled release of the incorporated drug, which then diffuses into the surrounding tissue as shown in Figure 10. The use of water-soluble materials is particularly advantageous, as it ensures predictable dissolution behavior after application. DMNs are widely used in vaccine delivery and have been investigated for protection against several infectious diseases, including malaria, influenza, hepatitis B, HIV, diphtheria, and polio. Compared with conventional hypodermic needles and other MN systems, they offer important benefits such as biocompatibility, scalable manufacturing, sufficient mechanical strength, and the elimination of biohazardous sharp waste after use, since the needle is not removed following insertion. Despite these advantages, their design and fabrication require a high level of technical expertise. In addition, effective performance depends on achieving full insertion of the MNs into the skin, which can sometimes be challenging. Another limitation is the time required for complete dissolution of the polymer matrix within the tissue. Nevertheless, their mechanism of action significantly reduces post-application risks, including needle-stick injuries, since no solid sharp structure remains after administration and the system is fully absorbed in situ [20,21,23,33,34].

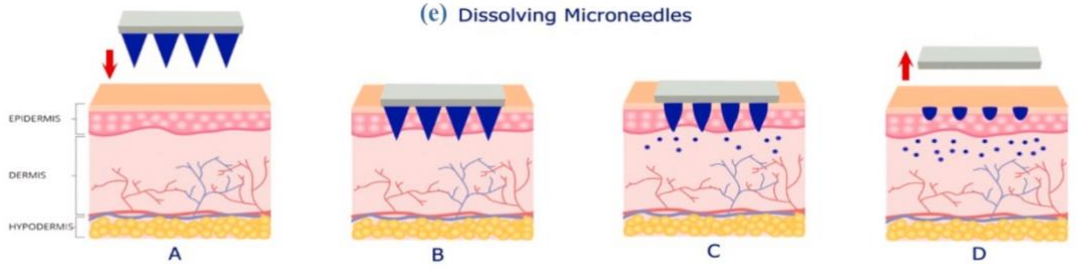

Figure 10: Dissolving MNs [34].

4.8.6 Stimuli-responsive MNs

Traditional MN drug delivery systems are generally classified as non-responsive systems, in which drugs are released through direct diffusion, particle degradation,

or matrix decomposition. Although these systems can provide therapeutic benefits, they deliver drugs independently of the surrounding physiological conditions and therefore cannot achieve controlled, on-demand release. This lack of adaptability may reduce therapeutic efficacy and increase the risk of side effects or drug overdose. To overcome these limitations, stimuli-responsive MNs (SR-MNs), commonly based on polymeric matrices, have recently attracted considerable attention as advanced transdermal drug delivery platforms [40]. These systems are designed to respond to specific environmental changes by mechanisms such as matrix swelling, degradation, dissociation, or cleavage, enabling a more precise and controlled release of therapeutic agents. Drug release can be triggered by internal physiological stimuli, including pH variations, glucose levels, redox conditions, and enzyme activity, or by external physical stimuli such as temperature, light, electric fields, ultrasound, magnetic fields, and mechanical stress. By exploiting pathological or physiological signals associated with the target tissue, SR-MNs provide space and time control over drug delivery, thereby improving therapeutic outcomes, improving delivery specificity, and reducing adverse effects related to off-target drug exposure [41].

4.9 FABRICATION TECHNIQUES

4.9.1 Laser Ablation

Laser ablation is a manufacturing technique that employs a focused laser beam to remove material from a substrate, enabling the fabrication of MN arrays, Figure 11. This approach has been extensively used in micro- and nanoscale processing for a wide range of technological applications. Various laser systems, such as CO_2 lasers, UV excimer lasers, and femtosecond lasers, have been explored for the production of MN structures. In this method, short laser pulses act as the energy source to selectively ablate portions of a solid material, typically requiring between 10 and 100 nanoseconds to reach the ablation threshold and shape the MN mold.

Laser ablation is generally considered a fast and efficient process, capable of producing high-aspect-ratio structures with relatively simple processing steps compared to techniques such as photolithography or dry etching. In particular, femtosecond laser systems, can further reduce processing time and maintenance requirements, lowering overall production costs. Additionally, this technique can yield MNs with favorable mechanical properties, including high tensile strength, and has been associated with improved drug permeability in transdermal delivery applications. It is also a non-contact process, which minimizes mechanical stress on the substrate and typically introduces a relatively low overall heat input. However, the localized thermal effects at the laser–material interface may still alter the microstructure and mechanical behavior of the fabricated MNs, potentially leading to defects such as micro-cracks or reduced fatigue resistance. Other limitations include the relatively high cost of equipment, restricted material compatibility, and the possibility of contamination or toxicity arising from laser–material interactions. Furthermore, despite its advantages, laser ablation is not always the most suitable option for large-scale mass production [20,21,33,42].

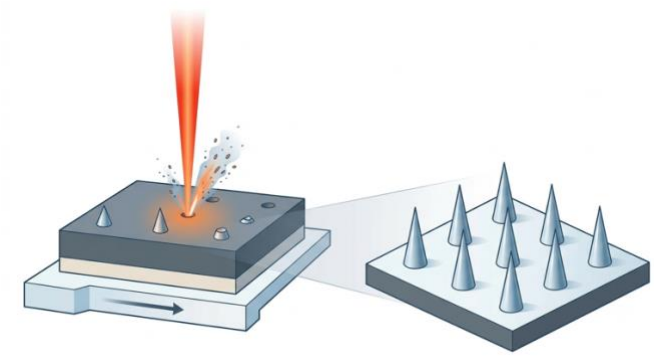

Figure 11: Representation of Laser Ablation technique, BioRender.

4.9.2 Lithography

The lithography technique is used to transfer a master geometric pattern onto a substrate surface. Among its variants, photolithography is the most commonly employed for pattern transfer due to its extensive use in microelectronics. Photolithography is a technique that uses light to transfer a predefined pattern from

a mask onto a photosensitive resist layer applied to a substrate. After this step, the substrate undergoes an etching process to eliminate undesired material, leading to the formation of the MN structure, Figure 12. The etching stage can be classified into two main categories, namely wet etching and dry etching, depending on the type of etchant used [43]. This method requires highly controlled processing of the photoresist material and represents a significant portion of manufacturing costs, accounting for roughly 30–35% of the total expense in integrated circuit production. Lithography can be applied to a wide range of materials, including glass, metals, ceramics, and polymers. It is also capable of producing highly accurate geometries with smooth, vertical sidewalls. However, the technique typically demands specialized cleanroom facilities and involves relatively long production times [20,21].

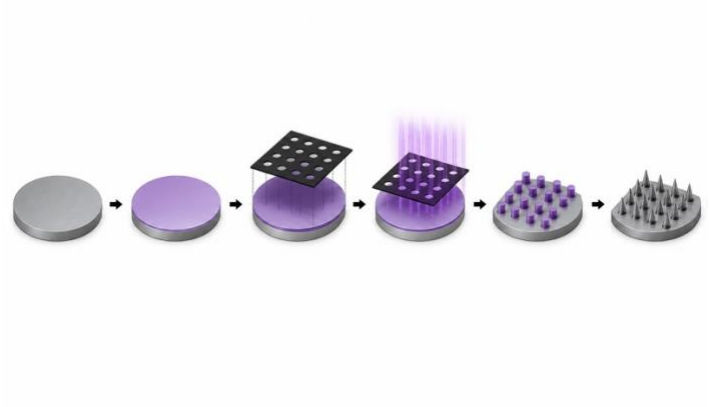

Figure 12: Representation of Lithography technique, BioRender.

4.9.3 Micromoding

The micromolding process involves creating replicas from a master mold. In this technique, the mold is filled with a solution composed of a polymer along with active pharmaceutical ingredients, Figure 13. Micromolding is generally regarded as a low-cost and scalable manufacturing approach, making it suitable for large-scale production. It is commonly applied using polymer-based materials for MN fabrication. Polydimethylsiloxane (PDMS) is frequently used in this process due

to several advantageous properties, including low cost, ease of handling, low surface energy, and good thermal stability. However, this method also presents certain limitations, such as challenges in precisely controlling insertion depth, restrictions in drug loading capacity, and variability in the mechanical performance of polymer-based MNs [20]. The advantages of this method lie in the relatively simple, cost-effective MN production at RT [21].

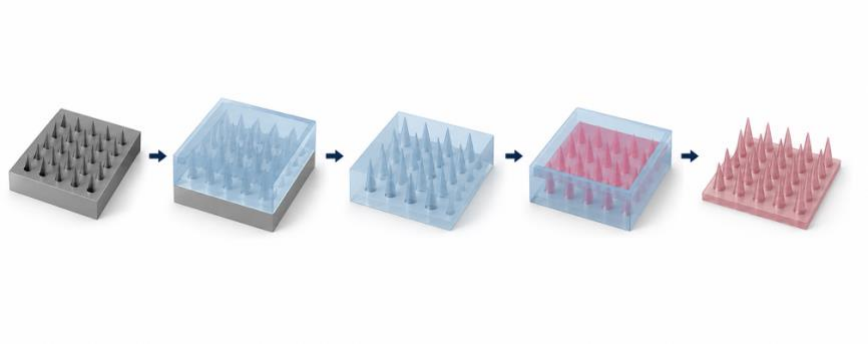

Figure 13: Representation of Micromolding technique, BioRender.

4.9.4 Injection molding

Microinjection molding is a fabrication technique that provides high repeatability, precise dosing, and rapid injection flow rates by separating the plasticization stage from the polymer melt injection process. These characteristics make it suitable for producing MN structures with consistent quality and performance. However, one of the main limitations of this method is the difficulty in controlling very small shot sizes, largely due to the typical screw dimensions, which are approximately 15–150 mm. In addition, the technique requires a relatively high initial investment in equipment, which can limit its accessibility [20].

4.9.5 3D printing

In recent years, additive manufacturing (3D printing) has attracted increasing interest as a method for producing MN arrays. A 3D printer constructs structures by depositing material layer by layer, enabling precise control over geometry as shown in Figure 14. In the biomedical field, these technologies have expanded rapidly, particularly in applications such as tissue engineering and implant

fabrication. In 2019, Johnson and colleagues developed the first MN master structure using a commercial 3D printer. Other studies have also employed stereolithography techniques to fabricate MN patches. One of the key advantages of 3D printing for MN fabrication is the high flexibility in design parameters, along with significantly reduced production times compared to conventional manufacturing methods [20]. Two primary 3D printing strategies are employed in the fabrication of MNs: material deposition and vat polymerization. Among material deposition techniques, the most widely used include fused deposition modeling (FDM) and material jetting (MJ). Vat polymerization, on the other hand, is a light-driven 3D printing method commonly applied to MN production. This category includes several techniques, such as stereolithography (SLA), digital light processing (DLP), continuous liquid interface production (CLIP), and two-photon polymerization (TPP) [44].

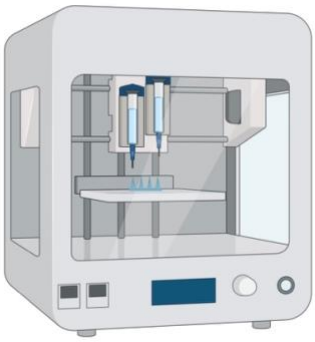

Figure 14: Representation of 3D printing technique, BioRender.

4.10 MATERIALS

The main objective behind the development of MNs is to create structures capable of penetrating the skin effectively without fracturing or deforming during application. To address the challenges associated with MN fabrication, several factors have been carefully investigated, including material selection, manufacturing techniques, and needle design. Numerous materials have been explored for the fabrication of various MN types, such as silicon, metals, ceramics, and polymers. In addition, combinations of different material classes have been

employed in biomedical applications, particularly in fields such as drug delivery, tissue engineering, and biomedical implant development.

4.10.1 Ceramic

Ceramics are materials composed of metallic and nonmetallic elements, where the interatomic bonds are predominantly ionic, often with some degree of covalent character. According to the American Ceramic Society, ceramics are inorganic, nonmetallic materials, typically crystalline, formed by combinations such as aluminum and oxygen (Al_2O_3), calcium and oxygen (CaO), or silicon and nitrogen (Si_3N_4). In recent years, ceramic MNs have attracted increasing attention due to their favorable properties [45]. Biocompatible ceramics offer high mechanical strength and excellent stability under conditions of elevated temperature and humidity, outperforming many polymer-based materials. They also allow controlled porosity and are relatively easy to handle during manufacturing. This tunable porosity, along with electrostatic interactions between the ceramic surface and permeating substances, can enhance transdermal drug delivery. Among the most used materials for ceramic MNs are alumina (Al_2O_3) and zirconia (ZrO_2), although calcium sulfate (in both hemihydrate and dihydrate forms) and calcium phosphate dihydrate have also been employed [20]. Alumina, in particular, is biologically inert and chemically stable due to the strong ionic and covalent bonds between aluminum and oxygen atoms. It exhibits good resistance under compressive forces and possesses higher fracture toughness compared to materials such as monocrystalline silicon. However, it is relatively brittle under tensile stress and requires high-temperature sintering during fabrication, which limits its compatibility with thermolabile drugs. Ceramic MNs can be produced using micro-molding techniques, a cost-effective method suitable for large-scale manufacturing. Despite their advantages, some limitations related to mechanical

performance, especially brittleness, have been reported, which may restrict their broader application [33,45].

4.10.2 Metals

Metals are widely used in the fabrication of MNs because of their excellent biocompatibility and favorable mechanical characteristics. They possess high fracture toughness as well as strong yield strength, making them more durable and resistant to breakage compared with silicon-based microneedles. A variety of materials are currently employed in the production of metallic MNs, including stainless steel, titanium, nickel, tungsten, palladium, tantalum, copper, and magnesium [46]. Stainless steel was the first metal employed in MN fabrication, followed later by titanium and other metallic materials. Due to their superior strength, metal MNs can effectively penetrate the skin without easily fracturing [47]. Despite these advantages, the use of metallic MNs may sometimes lead to allergic or hypersensitivity reactions in certain individuals [20].

4.10.3 Silicon

During the 1990s, the first MNs were manufactured using silicon as the primary material. Silicon offers several advantages compared with other materials, particularly its natural flexibility, which enables the fabrication of MNs in a wide range of shapes and dimensions. This material has been utilized in the production of solid, hollow, and coated MNs. However, despite these benefits, silicon also presents certain drawbacks. These include complex and time-intensive fabrication processes, relatively high production costs, and the risk of fracture during skin insertion, which may potentially leave broken fragments within the tissue [48].

4.10.4 Polymers

Over the past decade, polymers have emerged as highly promising materials for the fabrication of MNs, particularly in biomedical applications such as transdermal drug delivery and biofluid extraction. Their growing popularity in the medical field is largely due to their ease of processing, cost-effectiveness, and favorable biological and mechanical characteristics [20]. In particular, polymers are valued for their biocompatibility, low toxicity, biodegradability, and the possibility to tailor properties such as molecular weight and hydrophilicity. Polymeric materials offer several advantages, including flexibility and the ability to withstand significant bending without fracturing, making them tougher than many other MN materials, despite having lower tensile strength compared to metals and silicon [48]. They are widely used in the development of various MN systems, including dissolvable, hydrogel-forming, solid, coated, and hollow structures. Additionally, polymer-based MNs enable precise control over structure and functionality, allowing for the delivery of a broad range of therapeutic agents, from small molecules to larger biomacromolecules, often with sustained or controlled release profiles. A key advantage of biodegradable polymers is their ability to safely degrade in vivo into non-toxic byproducts, reducing the risk of infection or adverse effects in the event of needle breakage. Furthermore, their chemical versatility allows the incorporation of functional groups that can improve drug targeting and therapeutic efficacy while minimizing off-target effects. Polymeric MNs can also be fabricated without the need for complex micromachining techniques or cleanroom environments, simplifying large-scale production. However, some limitations remain. Biodegradable polymers may exhibit variable degradation rates, leading to challenges in controlling drug release and pharmacokinetics. In addition, non-biodegradable polymer fragments may persist in the skin if breakage occurs, potentially causing irritation or inflammation. Common polymers used in MN fabrication include polylactic acid (PLA), poly(lactic-co-glycolic acid)

(PLGA), cellulose acetate (CA), polyglycolic acid (PGA), polydimethylsiloxane (PDMS), polyethersulfone (PES), and polysulfone (PSF) [20,49].

4.11 BIOMATERIALS

4.11.1 Chondroitin Sulfate

Chondroitin sulfate (CS) is an anionic heteropolysaccharide belonging to the family of sulfated glycosaminoglycans (GAGs), a group of long linear polysaccharides composed of alternating amino sugars and hexuronic acids, Figure 15. It is one of the most abundant GAGs in the human body and is widely distributed in vertebrates, invertebrates, and certain bacteria. Structurally, CS consists of repeating disaccharide units of D-glucuronic acid (GlcA) and N-acetyl-D-galactosamine (GalNAc), linked through β-1,3 and β-1,4 glycosidic bonds. Sulfation can occur at different carbon positions, mainly at the C-4 or C-6 sites, generating several CS subtypes with variable sulfation patterns, chain lengths, and molecular weights, typically ranging from 50 to 100 kDa. Commercially, CS is commonly extracted from animal-derived tissues such as chicken cartilage, bovine trachea, porcine skin, nasal septum, and fish cartilage, contributing to its compositional heterogeneity [50]. CS is primarily found in the extracellular matrix (ECM), particularly in cartilage, bone, skin, tendons, ligaments, and blood vessels, where it plays a crucial role in maintaining tissue structure, repair, and regeneration. In articular cartilage, CS is especially important for cartilage homeostasis and recovery processes. Beyond its structural role, CS exhibits a broad range of biological activities, including antioxidant, anti-inflammatory, antiatherosclerotic, anticoagulant, antithrombotic, antiangiogenic, and neuroprotective effects [51].

Importantly, CS also shows significant immunomodulatory properties, as it can regulate inflammatory signaling pathways, influence cytokine production, and

modulate the activity of immune cells involved in tissue repair and chronic inflammation. Through these mechanisms, CS contributes to the attenuation of inflammatory responses and supports the restoration of tissue homeostasis in several pathological conditions, including osteoarthritis and other inflammatory diseases. In addition, CS is involved in neural signal transduction and may increase central nervous system activity [52]. It has also gained increasing attention in cancer therapy due to its ability to interact with CD44 receptors, making it a promising targeting molecule for drug delivery applications. The presence of hydroxyl and carboxyl functional groups in its structure allows easy chemical modification with hydrophilic or hydrophobic moieties, allowing the tuning of its physicochemical and pharmacological properties. Owing to its hydrophilic nature, CS can reduce non-specific interactions with serum proteins and prolong the circulation time of loaded or conjugated therapeutics. Alterations in CS levels have been associated with several pathological and physiological conditions, including osteoarthritis, inflammatory disorders, neurological diseases, aging, and cancer. Consequently, the development of CS replenishment and CS-based therapeutic strategies has become an important area of biomedical research [50,51].

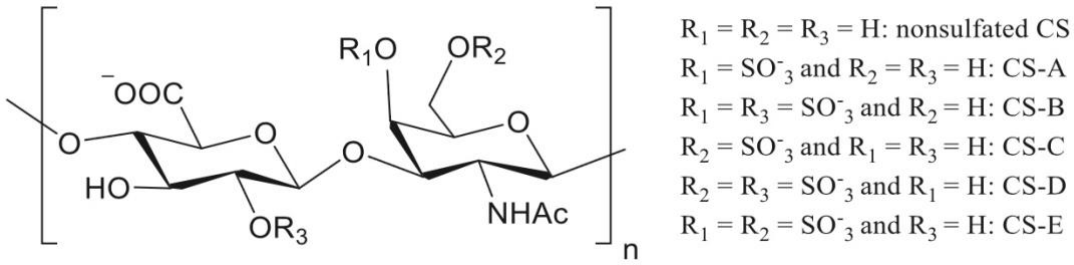

Figure 15: Chondroitin Sulfate chemical structure [50].

4.11.2 Dextran

Dextran (DEX) is a biocompatible, biodegradable, and non-toxic polysaccharide of microbial origin that was first discovered in 1874. Structurally, it is mainly composed of linear α-1,6-linked D-glucopyranose units with a small proportion of α-1,2-, α-1,3-, and α-1,4-linked side chains, Figure 16. DEX is naturally produced

by lactic acid bacteria such as *Leuconostoc mesenteroides* and can be synthesized from saccharose through the action of dextransucrase or from maltodextrins using dextrinase. In mammalian tissues, including humans, DEX can be enzymatically degraded by dextranase, further supporting its suitability for biomedical applications. Due to its hydrophilic nature, excellent biocompatibility, and ease of chemical modification, DEX has been extensively explored in pharmaceutical and biomedical fields, particularly in drug delivery systems and tissue engineering. Clinical grade dextrans with molecular weights of 40, 60, and 70 kDa are commonly used for these purposes [53]. Beyond biomedical applications, DEX has long been employed in the food industry because of its emulsifying, stabilizing, viscosifying, and texturizing properties [54]. In medicine, DEX is widely used to improve blood flow and reduce vascular thrombosis owing to its volume-expanding properties. It has also been shown to decrease inflammatory responses, limit ischemia–reperfusion injury during organ transplantation, and act as a mild reactive oxygen species scavenger capable of reducing excessive plaque activation. In emergency situations, soluble dextran complexes may also serve as temporary blood substitutes when compatible blood supplies are unavailable. Furthermore, DEX is frequently employed as a coating material to enhance the stability and biocompatibility of medical devices and nanocarriers [55].

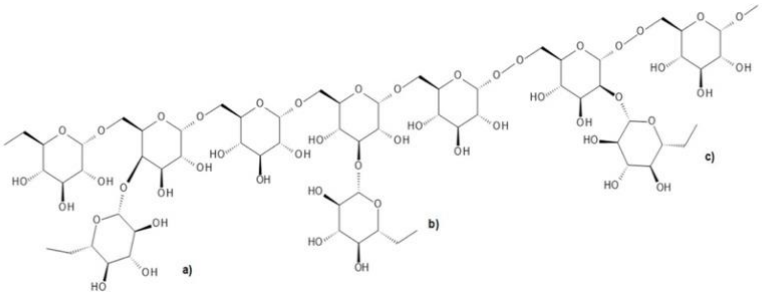

Figure 16: Dextran chemical structure [56].

4.11.3 Pullulan

Pullulan (PULL) is one of the most promising naturally derived polysaccharides and has recently attracted considerable interest because of its versatility in food, pharmaceutical, cosmetic, biomedical, and environmental applications. It is a microbial exopolysaccharide produced mainly by the yeast-like fungi *Aureobasidium pullulans* and *Aureobasidium melanogenum* under aerobic fermentation conditions using different carbon sources such as glucose, sucrose, inulin, xylose, and agro-industrial wastes. As a biologically derived and environmentally friendly polymer, PULL is biodegradable, edible, and considered generally recognized as safe (GRAS), making it highly attractive for commercial and biomedical use [57]. Structurally, pullulan is a homopolysaccharide composed of repeating maltotriose units, each containing three glucose molecules linked by α-(1→4) glycosidic bonds, while the maltotriose units themselves are connected through α-(1→6) linkages, Figure 17 [58]. This alternating arrangement of α-1,4 and α-1,6 glycosidic bonds generates a predominantly linear and flexible polymeric chain, contributing to its remarkable physicochemical properties. PULL generally exhibits a molecular weight ranging from approximately 4.5×10^4 to 6×10^5 Da and appears as a whitish or yellowish-white powder with a smooth surface morphology. The abundance of hydroxyl groups and its linear structure promote strong interactions with water molecules, giving PULL excellent water solubility even at low temperatures and enabling the formation of transparent and colorless aqueous solutions with concentration-dependent viscosity. Compared with many other polysaccharides, pullulan also displays relatively low viscosity, high thermal stability, and excellent film-forming ability. One of the most distinctive features of pullulan is its capacity to form robust, flexible, odorless, transparent, oxygen-impermeable, oleo-resistant, and edible films, fibers, and compression moldings. These properties arise from its unique molecular organization and adhesive behavior in aqueous environments. In addition to being

non-toxic, non-carcinogenic, non-mutagenic, and non-immunogenic, PULL demonstrates excellent biocompatibility, which further expands its potential in biomedical and pharmaceutical fields, particularly in drug delivery systems, tissue engineering, and wound-healing applications [59]. Owing to its outstanding chemical, biochemical, and physical characteristics, as well as the ease with which it can be chemically modified, PULL and its derivatives continue to gain increasing industrial relevance in areas including food technology, cosmetics, electronics, analytical sciences, energy production, and environmental remediation [57].

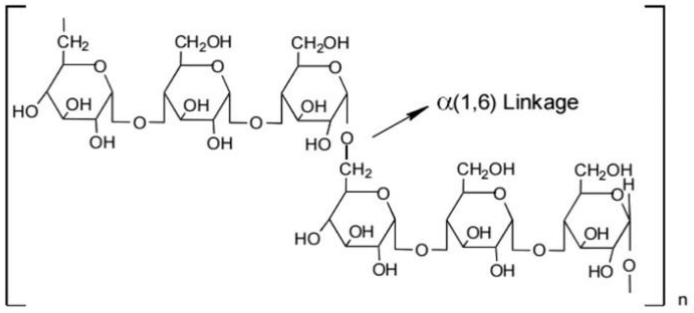

Figure 17: Pullulan chemical structure [57].

5. AIM

The aim of the present thesis was to develop and characterize DMNs intended for the intradermal delivery of an antigenic protein.

MNs are minimally invasive delivery systems composed of a microneedle array, which represent the functional portion of the device and can incorporate the active compound, and the backing layer that provides structural and mechanical support during both the application and the removal.

MNs are designed to penetrate the stratum corneum and reach only the most superficial layer of the skin, namely the epidermis and upper dermis, providing a minimally invasive, painless and bloodless administration while improving patient compliance.

The intradermal route was selected based on its immunological relevance. The skin contains a high density of antigen-presenting and other immunocompetent cells and may therefore promote an effective immune response even when relatively low antigen doses are administered. In addition, the limited mechanical disruption induced by MNs insertion may contribute to local immune activation.

From a clinical point of view this approach offers several advantages: the localized release minimizes its systemic distribution and also, compared with conventional syringe-based administration, DMNs exhibit high tolerability and ease of use, opening the potential of self-administration. In addition, the systems can provide simplified logistics (potentially overcoming cold-chain requirements) owing to the greater stability of the solid formulation.

Given these premises, chondroitin sulfate (CS) was combined with dextran (DEX) or pullulan (PULL) for the fabrication of innovative DMNs via micromolding assisted by solvent evaporation intended for the intradermal delivery of an antigenic protein.

The work focused on DMNs fabricated from biodegradable polymers, including CS, selected for its hydrophilic and potentially immunomodulatory properties, in combination with DEX or PULL. After insertion into the skin, the DMNs should be able to dissolve upon contact with interstitial fluids while releasing the antigenic protein in proximity to the immunocompetent cells.

The experimental work was divided into two main phases. In the first phase, polymeric formulations containing different concentrations of CS combined with either DEX or PULL were prepared and characterized using a rotational rheometer. The formulations were subsequently used to fabricate microneedles by micromolding in H600 PDMS molds. The resulting DMNs were characterized by scanning electron microscopy (SEM) for their morphological properties and by a texture analyzer in compression mode for their mechanical strength. This preliminary characterization allowed the selection of the four most promising formulations to be further characterized during the prosecution of the work. In the second phase, MN insertion capability was assessed using the Parafilm® insertion test. In addition, the rheological synergism of CS and DEX or PULL mixtures was investigated to better understand the interaction between the polymers employed. A dynamic mechanical analyzer (DMA) was then used to perform frequency-dependent compression tests on the DMNs in order to evaluate their viscoelastic mechanical behavior. Finally, the dissolution behavior of the DMNs was assessed thanks to the development of a biomimetic bilayer skin-mimicking hydrogel composed of agarose and gelatine using two different solvent mixtures for the two layers, in order to reproduce the different water content of stratum corneum and epidermidis. Such bilayer hydrogel thereby could provide insight into the dissolution behavior of the MNs under physiologically relevant conditions.

Thermal behavior, including Thermogravimetric analysis and Differential Scanning Calorimetry together with Fourier transform infrared spectroscopy analysis were carried out to investigate on DMNs solid-state and physical-chemical properties.

Finally, FITC-albumin was successfully incorporated into a selected DMNs formulation and its Recovery % was calculated by means of spectrofluorimetric analysis.

6. EXPERIMETAL PART

6.1 MATERIALS

Polymers

For the preparation of DMNs, the following materials were used: Chondroitin Sulfate (CS) (β-1,4-linked D-glucuronic acid and β-1,3-linked N-acetyl galactosamine) bovine 100 EP, low MW 14 kDa, mixture of chondroitin A (chondroitin 4 sulfate) and chondroitin C (chondroitin 6 sulfate) (batch number: 15/0008) from Bioiberica, Italy; Dextran (PM 500 kDa, batch number: DK424) purchased from Pharmacosmos, Denmark and Pullulan (batch number: 9F21) purchased from Hayashibara, Okayama. MilliQ water was used as solvent for the preparation of polymer solutions.

Biomimetic bilayer skin-mimicking hydrogel

For the preparation of the skin-mimicking hydrogel, Agarose (AG) (low electroendosmosis, batch number: 0000491933, Sigma-Aldrich, Spain) and gelatin (GEL) from porcine skin (gel strength 300, type A) were purchased from Sigma-Aldrich, United State of America.

Microneedles mold:

The MNs shape was obtained by means of a polydimethylsiloxane (PDMS) template (10x10, H600, B200, P500) purchased from Spring Applicator Micro, from Micropoint technologies Pte Ltd, Singapore.

6.2 METHODS

6.2.1 Polymer solution preparation

Solutions were prepared using chondroitin sulfate (CS) in combination with either dextran (DEX) or pullulan (PUL). Briefly, CS was gradually added to MilliQ water

under constant magnetic stirring at room temperature (RT) until complete dissolution. Subsequently, DEX or PUL was added to the CS solution and stirred until a homogeneous polymeric solution was obtained.

Different formulations were prepared by varying the concentration of CS and the secondary polymer. In the preliminary screening, CS was tested at concentrations of 40%, 30%, and 20% w/w, in combination with DEX or PUL at different concentrations (3.75 %, 5 %, 8 %, 10% w/w), as reported in Table 1.

After polymers dissolution, the solutions were sonicated for 30 min to promote degassing before microneedle fabrication.

Table 1: Quali-quantitative composition of MN-forming solutions. Concentrations are expressed as % w/w.

SOLUTIONS	CS	DEX	PUL
CS40DEX5	40	5	-
CS40PUL5	40	-	5
CS30DEX3.75	30	3.75	-
CS30PUL3.75	30	-	3.75
CS20DEX3.75	20	3.75	-
CS20PUL3.75	20	-	3.75
CS20DEX8	20	8	-
CS20PUL8	20	-	8

CS20DEX10	20	10	-
CS20PUL10	20	-	10

6.2.2 Rheological analysis

The rheological properties of the polymeric solutions were investigated using a rotational rheometer (MCR 102, Anton Paar,Italy) equipped with a CP50-1 cone plate. Viscosity measurements were performed at 25 °C, using a gap of 0.101 mm. Flow curves were obtained by applying increasing shear rates in the range 1–600 s^{-1}. All measurements were carried out in triplicate for each formulation. The viscosity profiles were reported as viscosity (Pa·s) as a function of shear rate (s^{-1}), in order to evaluate the flow behavior of the polymeric solutions and their suitability for the micromolding process. In addiction the rheological synergism of the solutions was calculated at three different shear rate according to the following Equation 1:

$$Rheological\ synergism = \frac{\eta mix}{\sum \eta}$$

η_{mix} = viscosity value of the polymeric mixtures (CS and DEX or PULL mixtures) prepared at different concentration.

$\sum \eta$ = sum of the viscosity values of CS solution and of secondary polymer (DEX or PULL) solution at the same concentration present in the mixture.

Figure 18: Rotational Rheometer Modular Compact Rheometer 102, Anton Paar s.r.l. Italy

6.2.3 Microneedles preparation

DMNs were prepared via micromolding technique followed by solvent casting. A PDMS mold containing a 10 × 10 array of pyramidal cavities, with a needle height of 600 μm, base width of 200 μm and pitch of 500 μm, was used. A graphical representation of MNs production process is reported in Figure 19.

Briefly, the PDMS template was placed and fixed inside a 50 ml Falcon tube and 200 μl of the polymeric solution was added onto the mold surface. The Falcon tube was then centrifuged for 5 minutes at 5.900 rpm to promote complete filling of the DMN cavities. This procedure was repeated five times to ensure homogeneous and complete filling of the mold. After the third centrifugation step, the excess solution remaining in the Falcon tube was recovered and reused instead of adding fresh polymeric solution.

The theoretical volume required to fill the DMN cavities was estimated according to the geometry of the mold. Since the MNs had a pyramidal shape, the volume of a single microneedle cavity was calculated using the following Equation 2 :

$$V_{MN} = \frac{1}{3}\, x\, b^2\, x\, h$$

where b is the base width of the MN cavity, corresponding to 200 μm, and h is the MN height, corresponding to 600 μm.

Therefore Equation 3 :

$$V_{MN} = \frac{1}{3} x\ (200\ \mu m^2)\ x\ 600\ \mu m = 8.0\ x\ 10^6\ \mu m^3$$

Since 1 µL corresponds to 10^9 µm³, the volume of one microneedle cavity was:

$$V_{MN} = 0.008\ \mu L$$

Considering the 10 × 10 array, corresponding to 100 MNs, the total cavity volume was Equation 4 :

$$V_{total} = 0.008\ \mu L\ x\ 100 = 0.8\ \mu L$$

Although the theoretical volume required to fill the DMNs cavities was approximately 0.8 µL, a higher volume of polymeric solution was used during the fabrication process to ensure complete mold coverage and efficient cavity filling during centrifugation.

After completion of the centrifugation steps, the mold was removed from the Falcon tube, and 100 µl of polymeric solution was deposited onto the surface of the mold to form the backing layer. The backing layer volume was selected to cover the whole patch area. Considering an 8 × 8 mm² patch area and an approximate backing layer thickness of 1 mm, the theoretical backing layer volume was calculated as follows Equation 5 :

$$V_{backing} = A\ x\ t = 8mm\ x\ 8mm\ x\ 1mm = 64\ mm^3$$

Since 1 mm³ corresponds to 1 µL:

$V_{backing}$ = 64 µL

Therefore, 100 µL of polymeric solution was added to ensure complete and homogeneous coverage of the backing layer.

The filled mold was left overnight under a chemical hood at RT to allow solvent evaporation. The following day, the dried DMN arrays were gently peeled off from the PDMS mold and stored under dry conditions until further analysis.

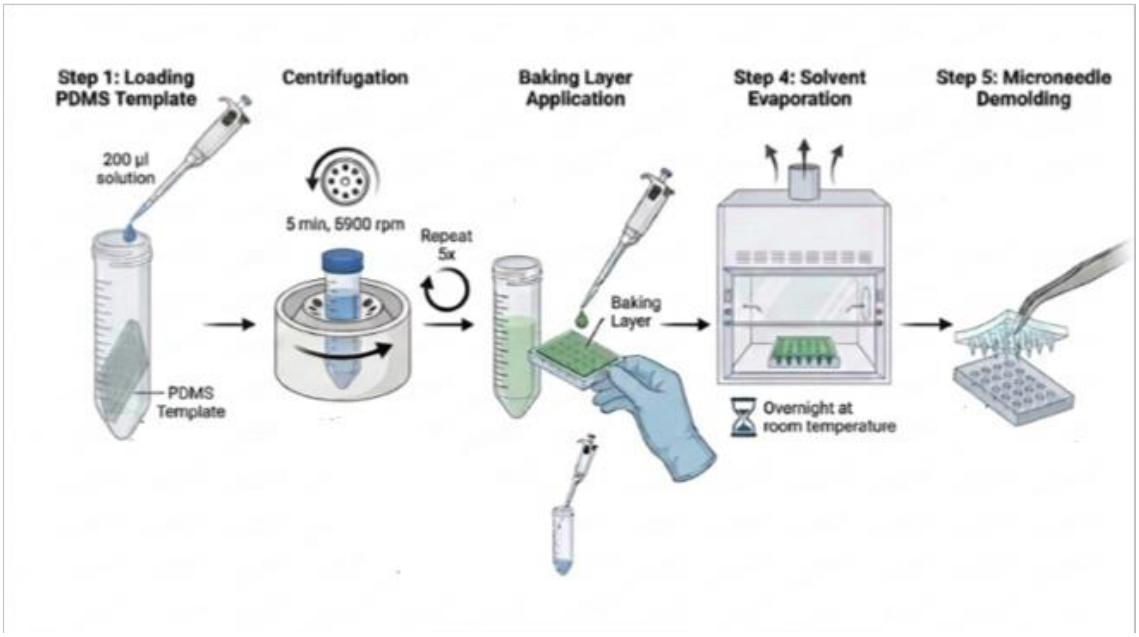

Figure 19: Graphical representation of MNs production process (FiguresLab).

6.2.4 Scanning Electron Microscope (SEM)

The morphological characterization of the DMN arrays was performed using a Phenom^{TM} Pure Desktop Scanning Electron Microscope (SEM) (ThermoFisher Scientific, Italy). Before analysis, the MNs were mounted on aluminum stubs and coated with a 20 nm gold layer using a Sputter Coater 208HR apparatus (United Kingdom), in order to improve sample conductivity. The coated samples were then and placed in the SEM chamber and observed under high-vacuum conditions at RT. Images were acquired at a magnification of 500x.

Figure 20: SEM Thermoscientific Phenom Pure (left) e Luxor Au sputter coater (right)

6.2.5 Static compression test

The DMNs mechanical properties were investigated in compression mode using a TA.XT plus Texture Analyzer (Stable Micro Systems, United Kingdom), equipped with a 10 kg cell and a 20 mm cylindrical probe (P/20P). The analysis was performed according to Fonseca et al. (2020) under the following conditions: pre-test speed of 1 mm/sec, test speed of 0.01 mm/sec, compression distance of 2 mm and a trigger force of 0.1 g. At least six replicates were carried out for each sample [60].

Force–time and Force/needle-time profiles were recorded during the compression test and reported. Moreover, after compression, the DMN arrays were further observed by SEM to evaluate possible deformation, fracture, or collapse of the needle structures.

Figure 21: TA.XT plus Texture Analyzer (Stable Micro Systems, United Kingdom) (BioRender).

6.2.6 Parafilm® insertion test

The insertion capability of the selected DMNs formulations was evaluated using a Parafilm® model, which is commonly employed as an artificial membrane to estimate DMNs penetration into the skin (Chen et al. 2022) [61]. Eight Parafilm® layers were stacked to obtain a total thickness of approximately 1.6 mm, with each layer corresponding to approximately 200 μm.

Each DMN array was placed on the first Parafilm® layer with the needle tip facing the membrane. The system was then positioned on the lower platform of a Texture Analyzer and compressed using a 20 mm cylindrical probe (P/20P); the method was adapted from Larrañeta et al. 2014 [62]. The test was carried out with a pre-test speed 1 mm/sec, test speed 0.01 mm/sec, and a penetration distance of 1.8 mm. Three replicates were performed for each sample.

After compression, the Parafilm® layers were carefully separated, and the number of holes produced by the MNs in each Parafilm® layer was counted.

Results are reported as the number of holes generated by each DMN as a function of Parafilm® layers and, consequently, Parafilm® layer depth, in order to compare the penetration capability of the different DMN formulations.

Moreover, the Penetration Rate % (PR %) was calculated for each layer according to the following Equation 6:

$$Penetration\ rate\ (PR\%) = \frac{number\ of\ holes\ created}{number\ of\ total\ needles}$$

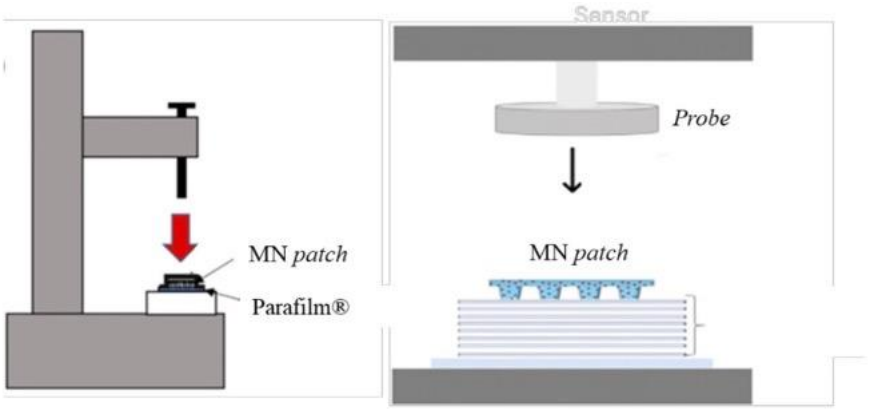

Figure 22: Illustration of MNs insertion test using TA.XT plus [62].

6.2.7 Dynamic Mechanical Analysis (DMA)

A Dynamic Mechanical Analyzer was employed to perform a compression test on the DMNs using a MCR 702e MultiDrive Dynamic Mechanical Analyzer (DMA) (Anton Paar, Austria). Measurements were carried out using a parallel-plate geometry, with a L-PAP50/TD/TS) as the lower plate and a PP25 as the upper plate.

First, an amplitude sweep test was performed in strain-controlled mode to identify the linear viscoelastic region (LVR) of each formulation. The test was performed at a constant frequency of 0.5 Hz, applying an extensional strain from 0.01 to 10%. Based on the amplitude sweep results, an extensional strain value corresponding to two-thirds of the LVR was selected to perform the subsequent oscillatory test, in order to avoid disruption of the sample structure during analysis.

Consequently, a frequency sweep test was carried out at the selected strain value over a frequency range of 0.5-10 Hz. For all formulations, the frequency sweep test was performed at a fixed extensional strain of 0.315%, which was within the LVR identified from the amplitude sweep analysis. The extensional storage modulus (E′), extensional loss modulus (E″), and loss factor (tan δ) were recorded.

The loss factor was calculated at 2.5 Hz as the ratio between E″ and E′, according to the following equation Equation 7 :

$$tan\ \delta = \frac{E''}{E'}$$

At least three replicates were performed for each DMN formulation.

6.2.8 Thermal behavior characterization

Thermogravimetric analysis (TGA) of the samples was performed using an STA 8000 instrument (PerkinElmer) under an inert nitrogen atmosphere, with a flow rate of 50 mL min^{-1}. The analyses were carried out in a platinum crucible over a temperature range from 30 °C to 1010 °C, at a heating rate of 5 °C min^{-1}. Differential scanning calorimetry (DSC) analysis was performed using a Q2000 instrument (TA Instruments). Approximately 6–8 mg of each sample was placed in an open aluminum crucible and analyzed under an inert nitrogen atmosphere, with a flow rate of 50 mL min^{-1}. Samples were heated from −40 °C to 300 °C and subsequently cooled to 25 °C at a rate of 5 °C min^{-1}.

6.2.9 Fourier Transform Infrared Spectroscopy analysis

Fourier transform infrared spectroscopy (FT-IR) analysis was performed using a FT-IR iS20 instrument (Nicolet, ThermoScientific, Italy). Physical mixtures and corresponding DMNs formulations were placed directly onto the ATR crystal and analyzed at room temperature. Spectra were recorded from 4000 to 400 cm^{-1}, with a spectral resolution of 4 cm^{-1}, by co-adding 64 scans for each sample. A background spectrum was collected before each analysis under the same experimental conditions. Spectra were expressed as Transmittance (%). For graphical comparison, the spectra were vertically offset without altering the position of the absorption bands.

6.2.10 Preparation of a biomimetic skin-mimicking model

A biomimetic skin-mimicking hydrogel was prepared to evaluate the dissolution behavior of the selected dissolving MN (DMNs) formulations under hydrated conditions. The model was designed as a bilayer hydrogel in order to reproduce, in a simplified manner, the different water contents of the stratum corneum and the viable epidermis. In particular, the upper layer was formulated to mimic the lower hydration level of the stratum corneum, while the lower layer was designed to reproduce the higher water content of the epidermal tissue.

The skin-mimicking hydrogel was prepared using 2% w/w agarose (AG) and 1% w/w gelatin (GEL) type A (Andree et al.2011, Zoudani et al.2025, Seow et al. 2019) [63–65] . Two different solvent mixtures were prepared using Dulbecco's Modified Eagle Medium (DMEM), as aqueous solvent mimicking the physiological conditions of the skin, and glycerol (GLY) to obtain different hydration levels. Glycerol was selected because it plays an important role in skin hydration, cutaneous elasticity and epidermal barrier repair [66]. The solution mimicking the stratum corneum consisted of 30% DMEM and 70% GLY, whereas the solution mimicking the epidermis consisted of 65% DMEM and 35% GLY. For each layer, the corresponding DMEM/GLY solution was heated under constant magnetic stirring at 85°C. AG was then gradually added and maintained under stirring until compete dissolution. Subsequently, the temperature was decreased to 60 °C, and GEL was added to the AG solution. The mixture was kept under stirring until complete GEL dissolution, obtaining a homogenous hydrogel precursor solution.

The bilayer hydrogel was then prepared by sequential casting into cylindrical glass molds ($\theta = 1$ cm). First, approximately 3 mL of the epidermis-mimicking solution was first poured into the mold and allowed to partially stabilize. Subsequently, 1 mL of the stratum corneum-mimicking solution was gently added on top to obtain

the upper, less hydrated layer. The hydrogels were then allowed to solidify at RT for 1 hour before use.

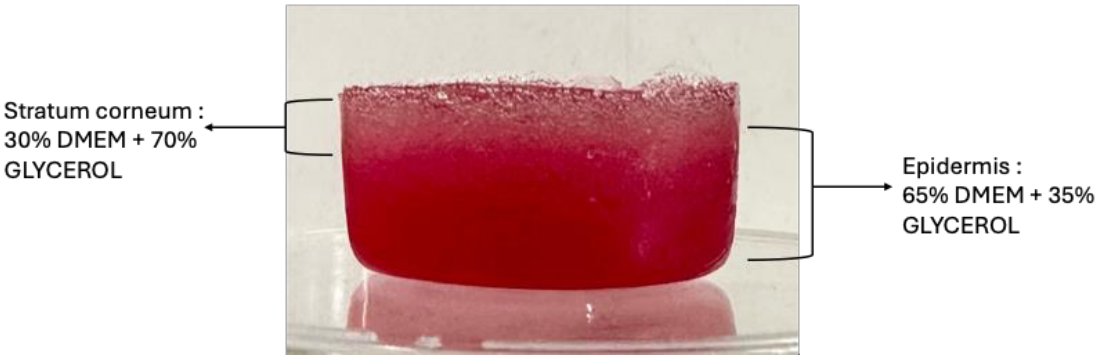

Figure 23: Composition of the two different layers of the skin mimicking AG/GEL hydrogel.

6.2.11 Dissolving test on biomimetic skin model

The dissolution behavior of the selected DMN formulations was evaluated using the biomimetic skin-mimicking hydrogel described in Section 6.2.10. To allow visual monitoring of the dissolution process, DMNs were prepared by adding methylene blue to the polymeric solutions before micromolding.

Each DMN array was inserted into the upper layer of the bilayer hydrogel using a dedicated MN applicator (Spring Applicator Micro, from Micropoint technologies Pte Ltd, Singapore). After application, the DMN arrays were maintained in contact with the hydrogel at RT for predetermined time intervals, namely 5, 10, 15, 20, 30, and 40 minutes. At each time point the DMN array was gently peeled off from the hydrogel in order to evaluate the progressive dissolution of the needle structure. Photographs of both the DMN array and the hydrogel surface after removal were acquired to visually assess changes in microneedle morphology and the release of methylene blue into the hydrogel.

The dissolution behavior was evaluated qualitatively by comparing the residual needle morphology at each time point. The progressive reduction in needle length

and the diffusion of methylene blue within the hydrogel were used as visual indicators of DMN dissolution and polymer release under hydrated conditions.

6.2.12 Loading of FITC-Albumin as protein model

FITC-albumin was incorporated into a 20% CS and 8% dextran DMNs at a final concentration of 2 mg/mL (0.2% w/w). Since FITC is photosensitive, all procedures were carried out under light-protected conditions using amber vials. Two polymeric solutions were prepared for the fabrication of DMNs. The first solution, containing only the polymeric matrix, was used for the fabrication of the backing layer. The second solution was supplemented with FITC-albumin to obtain the desired final concentration and was used to fill the MNs mold cavities. Based on the formulation composition (20% CS, 8% dextran and 0.2% FITC-albumin), it was possible to calculate their theoretical dry composition:

Total % composition:

Equation 8:

$$\text{CS} + \text{DEX} + \text{FITC-albumin} : 20 + 8 + 0.2 = 28.2\ \%$$

Equation 9:

$$CS: \left(\frac{20}{28.2}\right) x\ 100 = 70.9\%$$

Equation 10:

$$DEX: \left(\frac{8}{28.2}\right)\ x\ 100 = 28.4\%$$

Equation 11:

$$FITC - Albumin: \left(\frac{0.2}{28.2}\right)\ x\ 100 = 0.71\%$$

Accordingly, a microneedle array with an average dry weight of approximately 30 mg was expected to contain about 213 μg of FITC-albumin.

6.2.13 Spectrofluorimetric analysis

FITC-albumin loading into DMNs was evaluated by means of a spectrofluorimetric analysis. Individual MNs arrays (average weight: approximately 30 mg) were weighed and dissolved in 1 mL of phosphate-buffered saline (PBS, pH 7.4). Samples were protected from light throughout the procedure and incubated at RT or at 37°C until complete dissolution of the polymeric matrix. The resulting solutions were gently centrifugated to remove any undissolved material. The supernatants were collected for fluorescence analysis. FITC fluorescence was measured using a spectrofluorometer and black 96-well microplates, with excitation and emission wavelengths of approximately 485–495 nm and 515–525 nm, respectively. Before the analysis samples were diluted 1:10 in PBS. Quantification was performed using a calibration curve prepared from FITC-albumin standard solutions in PBS at concentrations of 0.5, 1, 2.5, 5, 10, 25, and 50 μg/mL, obtained by serial dilution of a stock solution. The linearity of the calibration curve was assessed by linear regression analysis and resolution of the coefficient of determination (R^2) (Figure 24).

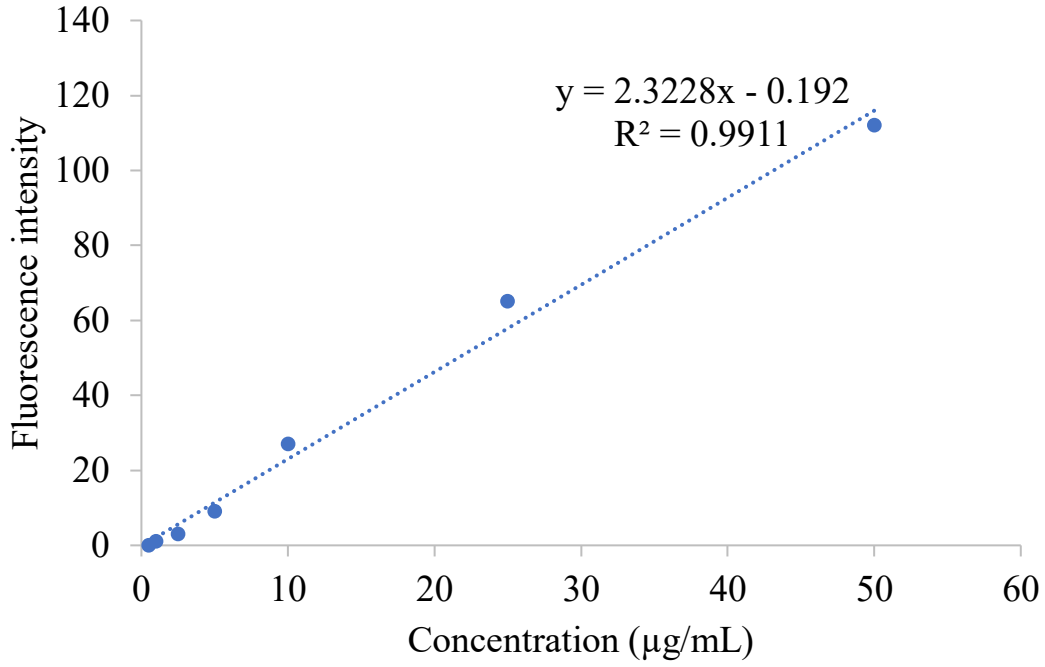

Figure 24: Calibration curve of FITC-albumin

To account for the intrinsic fluorescence of the polymeric matrix, fluorescence values obtained from blank MNs (without FITC-albumin) processed under identical experimental conditions were subtracted from those of FITC-loaded samples. FITC-albumin concentration was determined by interpolation from the calibration curve. The recovery efficiency was calculated according to the following equation:

Equation 12:

$$\text{Recovery}(\%) = \frac{\text{FITC-albumin measured after MN dissolution}}{\text{Theoretical FITC-albumin loading}} \; x \; 100$$

6.2.14 Evaluation of FITC-Albumin diffusion in AG/GEL skin-mimicking model

DMNs loaded with a FITC-albumin were fabricatd to evaluate the dissolution of the selected DMNs and the release of an encapsulated model protein. Two formulations were prepared: one containing FITC-albumin encapsulated within the MN tips and a second containing FITC-albumin combined with methylene blue

within the MN tips. Methylene blue was added to allow the visualization of polymers dissolution. Backing layer was composed in both cases only by the polymers mixtures.

MN arrays were inserted into a AG/GEL skin mimicking hydrogel prepared as described in 6.2.10, using a dedicated MN applicator (Micropoint technologies Pte Ltd, Singapore) to ensure a standardized insertion depth and application force. Following insertion, the dissolution of the MNs and the release of FITC-albumin into the hydrogel matrix were monitored over time by confocal laser scanning microscopy (CLSM, Leica TCS SP2, Leica Microsystems, Italy). Sequential optical images were acquired at predefined time points to visualize the progressive dissolution of the MNs tips, with the help of the methylene blue, and to assess the spatial distribution and diffusion of FITC-albumin within the hydrogel due to its fluorescence.

6.2.15 Cell culture management

Normal Human Dermal Fibroblast (NHDF) and RAW 264.7 macrophages (VWR, Italy) cells were cultured in polystyrene tissue culture flasks (Cellstar® Tissue Culture Flasks, Greiner Bio-One, Italy) using complete culture medium (CM), consisting of high-glucose Dulbecco's Modified Eagle Medium (DMEM) supplemented with 10% v/v fetal bovine serum (FBS), previously heat-inactivated in a thermostatic water bath at 56 °C for 30 min, and 1% v/v of a 100× penicillin/streptomycin/amphotericin solution.

Cells were maintained in a CO_2 incubator (PBI International, Italy) at 37 °C, 95% relative humidity, and 5% CO_2. Cell morphology and growth were monitored daily using an inverted optical microscope.

When cells covered 80% of the available growth surface, the culture was considered confluent. At confluence, cell proliferation decreased due to contact

inhibition; therefore, cells were detached from the plastic surface and subcultured into new flasks.

6.2.16 Cell trypsinization

Cell trypsinization was performed whenever the cells reached approximately 80% confluence, in order to detach them from each other and from the culture surface. After confirming cell confluence and morphology, the culture medium was removed and the cell monolayer was washed with phosphate-buffered saline (PBS). The PBS was then aspirated, and a trypsin solution was added to the flask. Trypsin is a proteolytic enzyme that promotes cell detachment by degrading proteins involved in cell–cell and cell–substrate adhesion. To promote enzymatic detachment, the flask was incubated at 37 °C for 5 min.

Once the cells had detached, CM was added at twice the volume of the trypsin solution to inhibit enzymatic activity. The cell suspension was transferred into a centrifuge tube and centrifuged at 1500 rpm for 5 min using a Sorvall TC6 centrifuge (Sorvall Products, United State of America).

After centrifugation, the supernatant containing trypsin was carefully removed without disturbing the cell pellet. The cells were then resuspended in complete culture medium, counted, and seeded into one or more new flasks. Each trypsinization procedure was considered one cell passage.

The same procedure was used both for routine cell subculturing after reaching approximately 80% confluence and for cell detachment before experimental procedures.

6.2.17 Cell counting

The number of cells in suspension was determined using a hemocytometer (Hycor Biomedical, United State of America). An aliquot of the cell suspension was mixed at a 1:1 ratio with a 0.05% w/v Erythrosin B (Sigma Aldrich, Italy) solution and

then transferred into the counting chamber. Erythrosin B is a viability dye that is taken up only by cells with damaged membranes; therefore, dead cells appear pink, whereas viable cells remain unstained

Cells were observed using an inverted optical microscope, and only viable, unstained cells were counted. The total number of viable cells in suspension was calculated according to the following Equation 13:

$$\left(\frac{n° \; of \; cells}{n° \; of \; squares}\right) \cdot 2 \cdot 10000 \cdot V$$

where n° of cells is the number of viable cells counted, n° of squares is the number of chamber squares analyzed, 2 is the dilution factor, 10^4 is the chamber volume correction factor, and V is the total volume of the cell suspension, expressed in mL.

6.2.18 In vitro cytotoxicity assessment

The cytotoxicity of the MNs was evaluated using normal human dermal fibroblasts (NHDFs) and murine RAW 264.7 macrophages.

Before contact with the cells, the MNs were exposed to ultraviolet radiation (3 cycles of 20 minutes). MNs were then solubilized in CM and four concentrations were tested for each formulation namely 30 mg/ml, 22.5 mg/ml, 15 mg/ml and 10 mg/mL. The solutions were then filtered with a 0.22µm (CA Syringe Filter, ClearLine®) filter before usage with cells.

Both cell lines were seeded into 96-well tissue culture plates (Corning® 96-Well TC-Treated Microplates) at a density of 17,500 cells/well, corresponding to approximately 50,000 cells/cm², and incubated for 24 h at 37 °C in a humidified

atmosphere containing 5% CO_2. After incubation, the culture medium was removed and replaced with 100 µL of MNs solutions. Cells maintained in CM were used as the control. After a further 24 h of exposure, cell viability was evaluated using the AlamarBlue assay.

6.2.19 AlamarBlue assay

The AlamarBlue assay was used to evaluate cell viability based on the reducing activity of metabolically active cells, providing a quantitative estimation of cell proliferation and cytotoxicity.

The assay is based on resazurin, a non-toxic, cell-permeable compound that is blue and weakly fluorescent in its oxidized form. In viable cells, resazurin is reduced to resorufin, which is pink and highly fluorescent. Therefore, the amount of resorufin produced is directly related to the metabolic activity and viability of the cell population.

After 24 h of treatment, the culture medium was removed from NHDFs and RAW 264.7, and 100 µL of a 10% v/v AlamarBlue (Thermofisher, Italy) solution prepared in phenol red-free DMEM was added to each well. The 96-well plate was then incubated for 3 h at 37 °C.

At the end of the incubation period, fluorescence was measured using a multimode microplate reader (FLUOstar Omega Microplate Reader, BMG Labtech, Germany) at an excitation wavelength of 540 nm and an emission wavelength of 590 nm. Cell viability % was calculated by comparing the fluorescence intensity of treated samples with that of untreated control cells (CM).

7. RESULTS AND DISCUSSION

The experimental work initially focused on the preparation and rheological characterization of different polymeric solutions based on chondroitin sulfate (CS) in combination with either dextran (DEX) or pullulan (PULL).

Rheological analysis was performed as a preliminary screening step, since viscosity represent a critical parameter for micromolding-based MN fabrication, as this parameter strongly influences the filling of the PDMS molds. In fact, the occurrence of shear-thinning behavior of the MN-forming solution is required to allow the solution to efficiently flow into the mold cavities during centrifugation while maintaining sufficient consistency, in order to form well-defined MNs after solvent evaporation [67]. Specifically, the viscosity must be sufficiently low to allow complete cavity filling while remaining high enough to prevent defects during the molding process [69].

Results of the rheological characterization are reported in Figure 25 corresponding to CSPULL formulations and Figure 26 to CSDEX formulations.

The first formulations investigated were composed of 40% w/v CS combined with 5% w/v DEX or 5% w/v PULL. Both solutions exhibited a pseudoplastic, or shear-thinning, behavior, characterized by a progressive decrease in viscosity with increasing shear rate. In detail, among these formulations, the PULL-containing solutions showed slightly higher viscosity than the corresponding DEX-based formulation.

However, the relatively high viscosity of the 40% w/v CS formulations could potentially hinder efficient mold filling. Therefore, the concentration of CS was reduced to 30% w/w, while the concentration of DEX or PULL was proportionally decreased to 3.75% w/v. Under these conditions, the viscosity profiles of the DEX- and PULL-containing formulations became comparable and, moreover, both

solutions showed lower viscosity values compared with the 40% CS-containing formulations.

A further reduction of the CS concentration to 20% w/w, while maintaining DEX or PULL at 3.75% w/v, resulted in a marked decrease in viscosity for both formulations. Although this reduction improved solution fluidity, the viscosity appeared too low to ensure optimal formulation performance during MN fabrication. For this reason, the concentration of the secondary polymer was increased to 8% w/w. This adjustment led to an increase in viscosity in both DEX- and PULL-based formulations. In particular, the viscosity of the CS20DEX8 formulation remained lower than that of the corresponding CS30DEX3.75 formulation, whereas the CS20PULL8 formulation showed a viscosity profile comparable to that of the CS30PULL3.75 system.

A similar trend was observed when the concentration of DEX or PULL was further increased to 10% w/w. In detail, the PULL-based formulations exhibited higher viscosity values than the corresponding DEX-based formulation, suggesting a stronger contribution of PULL to the overall rheological behavior of the polymeric solution or the eventual occurrence of interactions between the components.

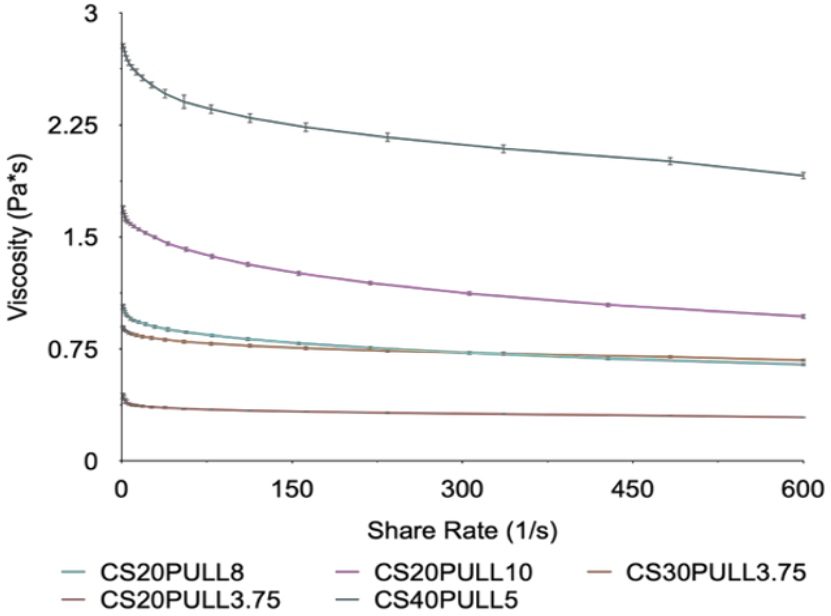

Figure 25: Viscosity profile of CSPULL DMNs

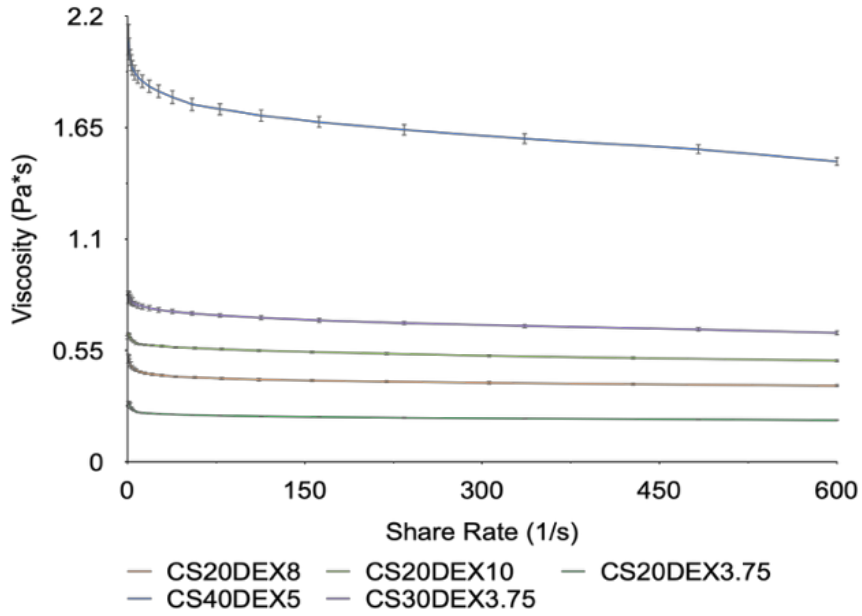

Figure 26: Viscosity profile of CSDEX DMNs

After the preliminary rheological screening, the prepared solutions were used to fabricate MNs through the micromolding technique as described in Section 6.2.3. Once dried and removed from the PDMS molds, the MN arrays were analyzed by

scanning electron microscopy (SEM) to evaluate their morphology, mold-filling efficiency, tip formation, and the presence of possible structural defects. SEM photomicrographs are reported in Figure 27.

SEM analysis revealed clear differences in MNs morphology as a function of the formulation composition. For the formulations 40% w/w CS with 5% w/w DEX or PULL, the MNs were successfully formed; however, they exhibited an uneven morphology, and the needle tips were not completely filled. This behavior may be related to the relatively high viscosity of these formulations, which could limit the efficient filling of the mold cavities during centrifugation.

A similar morphology was observed after reducing the CS concentration to 30% w/w and DEX or PULL concentration to 3.75% w/w, while maintaining the same polymer ratio. Although defined MNs were obtained, the arrays still showed morphological heterogeneous, with partially incomplete or poorly formed needle tips.

When the CS concentration was further reduced to 20% w/w while maintaining DEX or PULL at 3.75% w/w, a slight improvement in MN morphology was observed. Nevertheless, the needle tips remained partially incomplete or fractured, indicating that the formulation was still not optimal for producing homogenous and well-defined MN arrays.

Finally, the formulations containing 20% w/w CS combined with 8% or 10% w/v DEX or PULL allowed the formation of MNs with a more homogeneous morphology and well-defined, completely filled needle tips. No substantial morphological differences were observed between the DEX or PULL based formulations at these concentrations. These results suggest that increasing the concentration of the secondary polymer improved the ability of the formulations to form structurally complete DMNs after solvent evaporation. Among the

investigated formulations, CS20DEX8, CS20DEX10, CS20PULL8, and CS20PULL10 showed the most suitable morphology, characterized by homogeneous arrays and complete needle-tip formation.

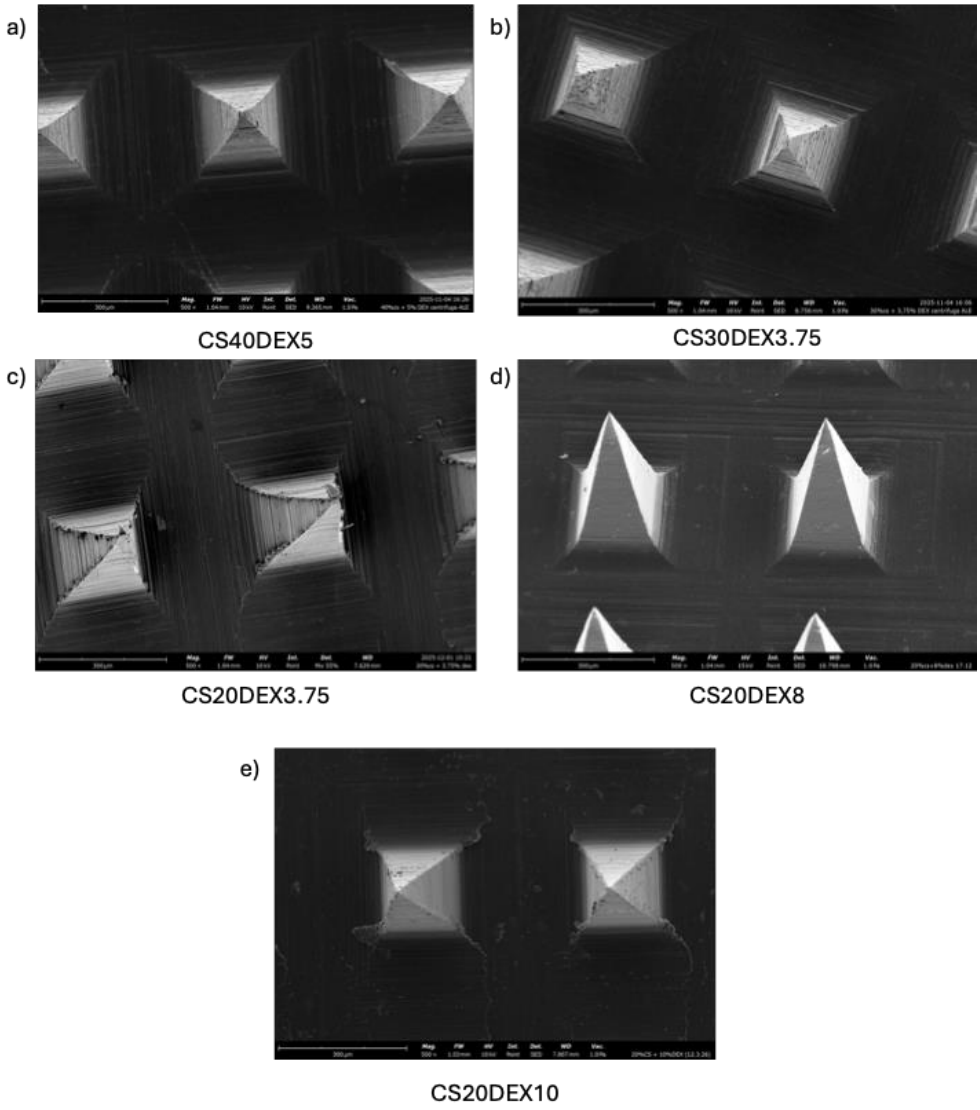

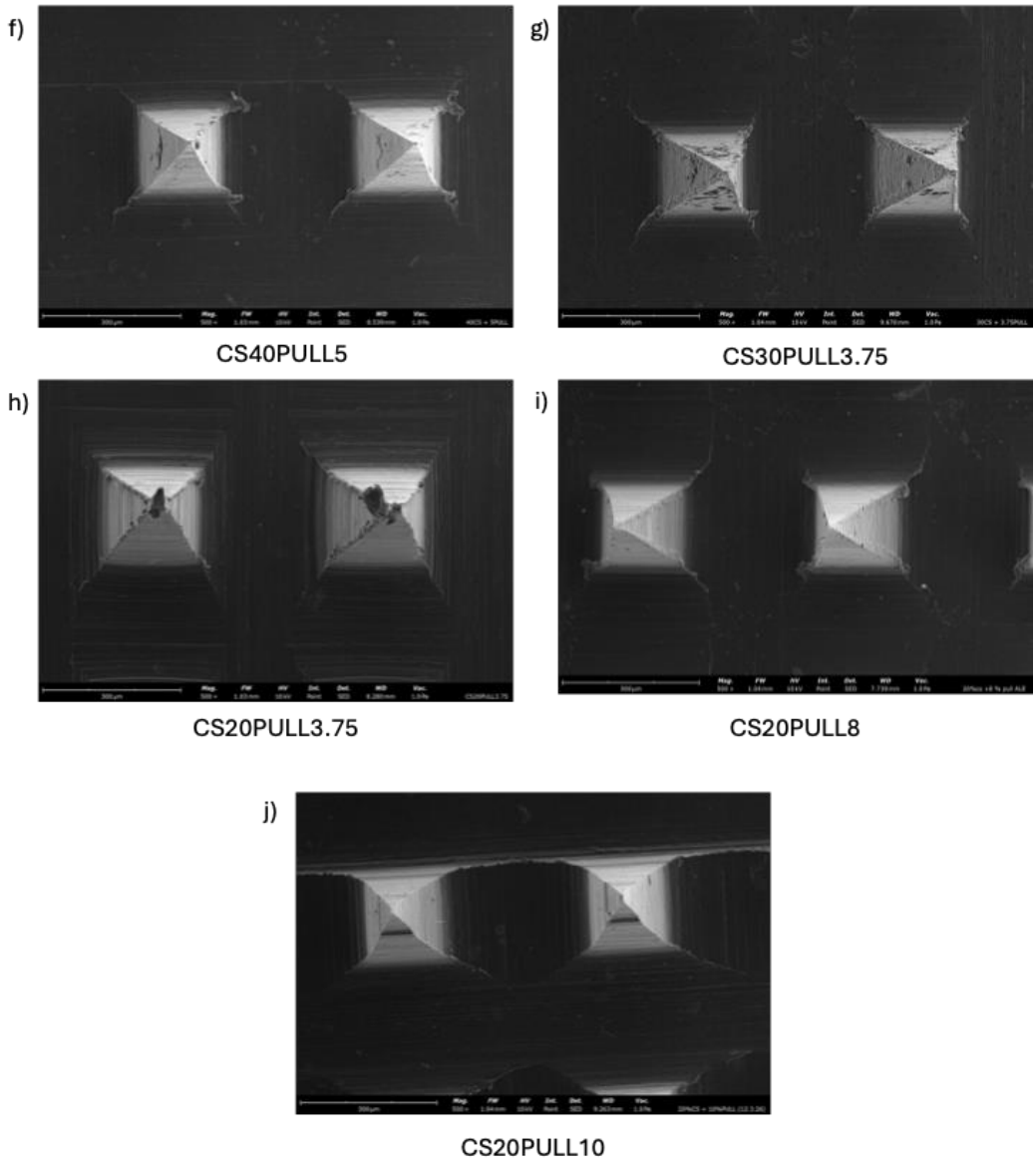

Figure 27: SEM images of a) CS40DEX5, b) CS30DEX3.75, c) CS20DEX3.75, d) CS20DEX8, e) CS20DEX10, f) CS40PULL4, g) CS30PULL3.75, h) CS20PULL3.75, i) CS20PULL8, j) CS20PUL10 MNs at 500x magnification.

Besides morphology, the mechanical strength of the MNs represents another critical parameter, as the needles must be able to penetrate the stratum corneum without bending or fracturing during application [68].

For this reason, the different formulations were analyzed in axial compression mode using a Texture Analyzer, as described in Section 6.2.5**Error! Reference**

source not found.. As can be observed from the graphs, all formulations showed a progressive increase in Force during compression, indicating their ability to resist the applied load. However, differences were observed depending on the polymer composition. As expected, formulations with higher polymer content reached higher force values, suggesting greater stiffness and resistance to compression. Nevertheless, these results could suggest a more brittle behavior, which may could affect MNs performance during application.

Interestingly, CS20DEX8, CS20DEX10, CS20PULL8, and CS20PULL10 MNs showed the best compromise between brittle and elastic/plastic behavior among all the formulations.

The results are reported Figure 28 and Figure 29 showing Force (N) vs Time (s) profiles for DEX- and PULL-based MNs respectively.

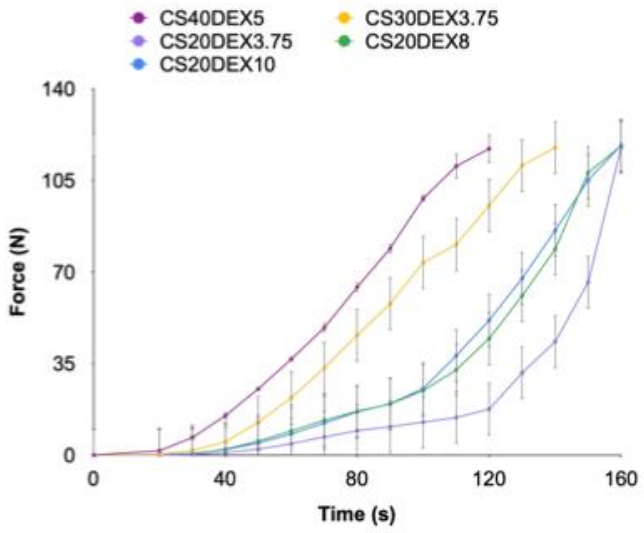

Figure 28: : Force (N) vs Time (s) profiles recorded for CSDEX-based DMNs. Data are expressed as mean values ± sd, n=6.

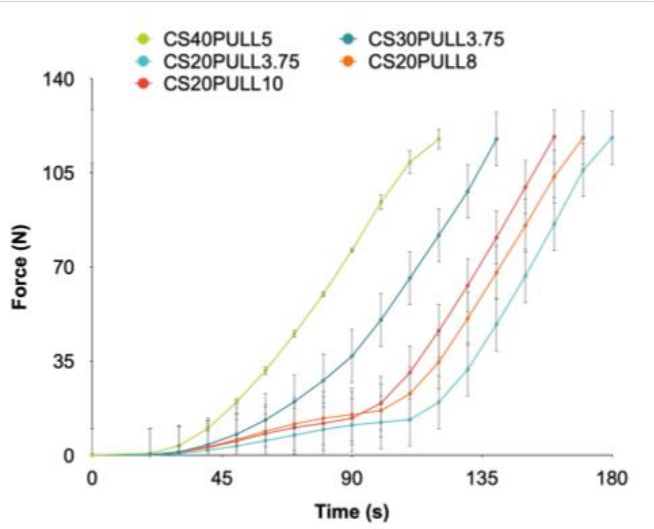

Figure 29: Force (N) vs Time (s) profiles recorded for CSPULL-based DMNs. Data are expressed as mean values ± sd, n=6.

Moreover, after mechanical testing, MNs arrays were subjected to SEM analysis in order to evaluate their morphological properties after being subjected to compression. SEM microphotographs are reported in Figure 30.

The post-compression SEM images supported these observations. Among the tested formulations, CS20DEX8, CS20DEX10, CS20PULL8, and CS20PULL10 showed the best structural integrity, with limited deformation and no evident collapse of the needle structures after mechanical testing. These formulations provided the best compromise between complete mold filling, homogeneous MN morphology, and adequate mechanical performance.

In contrast, the other formulations displayed more pronounced damage, including fractured or poorly preserved tips. These observations could confirm the more brittle mechanical behavior of these formulations, despite the higher compressive forces reached by some of them during testing.

Overall, the compression test showed that polymer composition strongly affects the mechanical behavior of DMNs.

a)

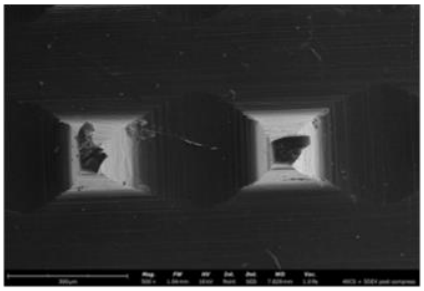

CS40DEX5

b)

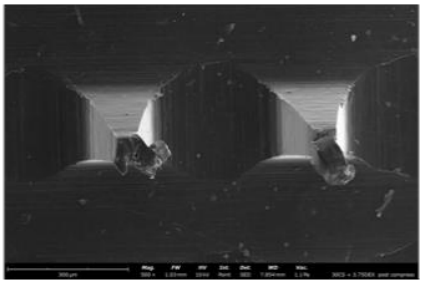

CS30DEX3.75

c)

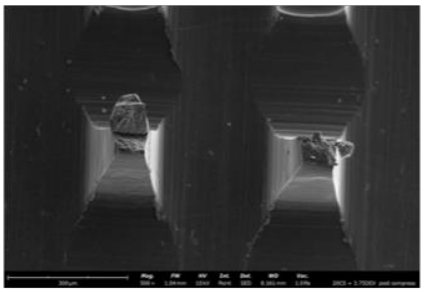

CS20DEX3.75

d)

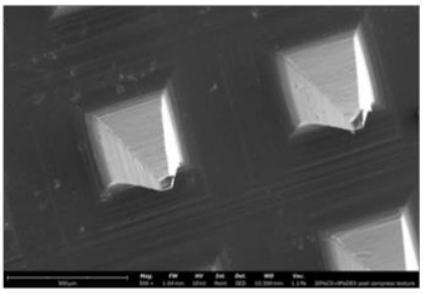

CS20DEX8

e)

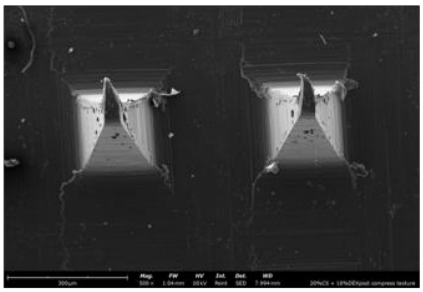

CS20DEX10

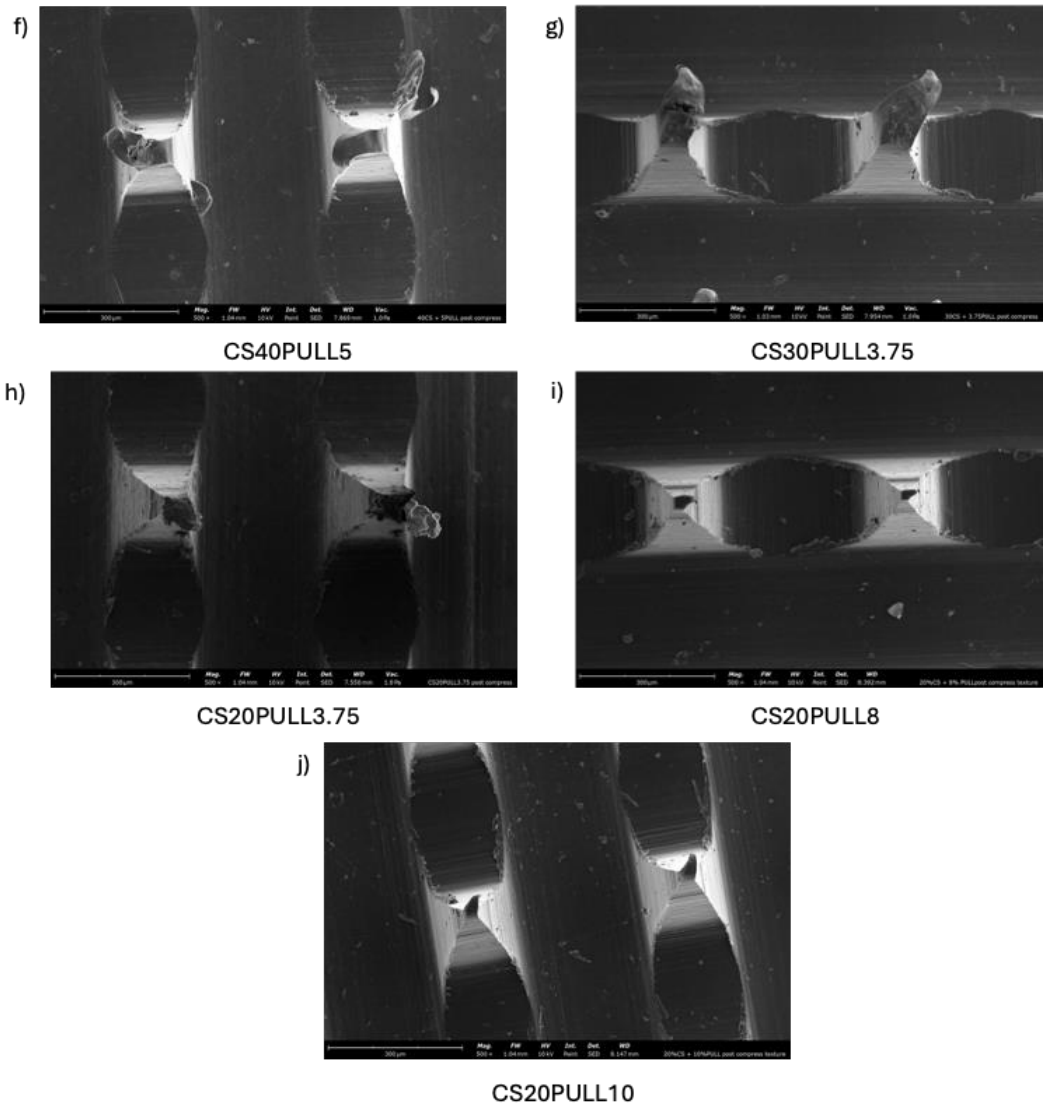

Figure 30: : SEM images of a) CS40DEX5, b) CS30DEX3.75, c) CS20DEX3.75, d) CS20DEX8, e) CS20DEX10, f) CS40PULL4, g) CS30PULL3.75, h) CS20PULL3.75, i) CS20PULL8, j) CS20PULL10 MNs after axial compression at 500x magnification.

Based on both morphological and mechanical results, the four formulations CS20DEX8, CS20DEX10, CS20PULL8, and CS20PULL10 were selected for further characterization.

According to the literature, a minimum insertion force of approximately 0.15 N per needle is required to successfully penetrate the stratum corneum without distortion [62] and a minimum insertion force of 0.058 is needed to break the

surface layer of the skin [68]. For this reason, Force/needle (N) values were calculated for the selected formulations; Force/needle (N) vs Time (s) profiles are reported in Figure 31. As can be observed from the graph, all formulations successfully exceeded both values, suggesting their feasibility for skin insertion.

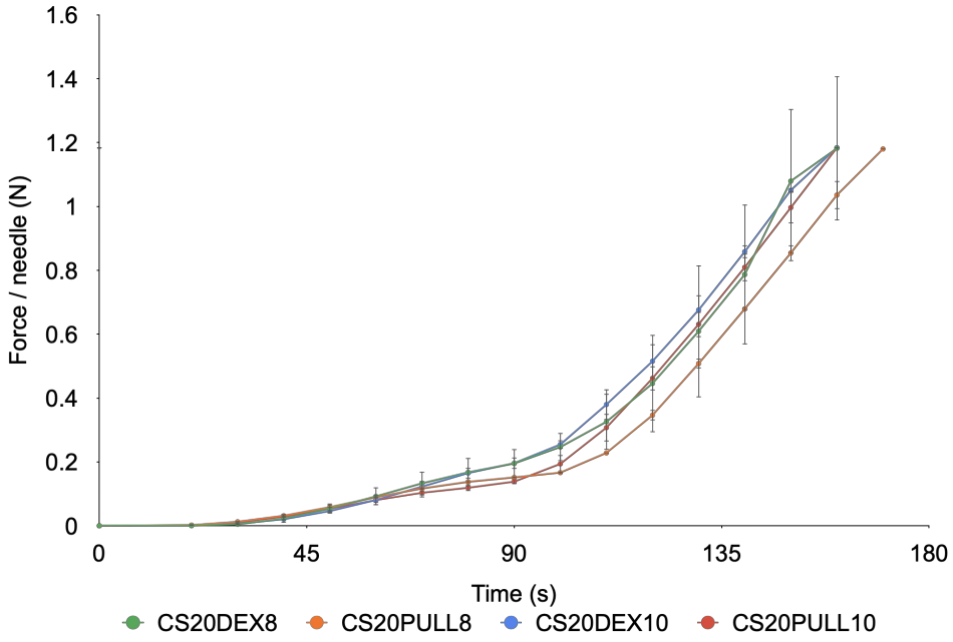

Figure 31:: Force/needle (N) vs Time (s) profiles recorded for CS20DEX8, CS20DEX10, CS20PULL8, CS20PULL10 DMNs. Data are expressed as mean values ± sd, n=3.

After the morphological and mechanical testing, a more detailed rheological characterization was performed on the previously selected formulations with the aim of investigating whether synergistic rheological interactions occurred between the polymers. First, the viscosity of the individual polymer solutions was evaluated and then compared with that of the corresponding mixed formulations. Results are shown in Figure 32 a) and b).

In particular, it can be noticed that when CS was combined with DEX or PULL, the viscosity of the mixed formulations was considerably higher than that of the

individual polymer solutions. This suggested the presence of a positive rheological synergism between CS and the second polymer.

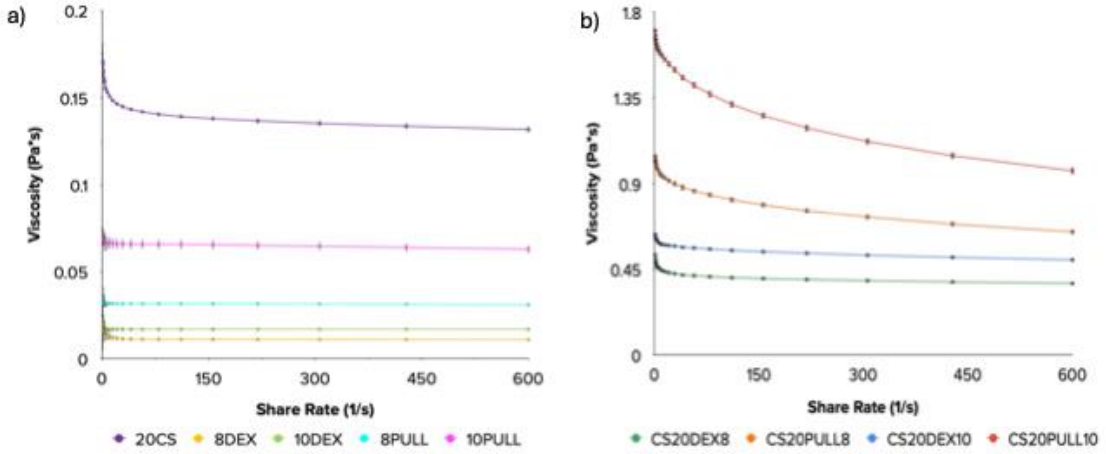

*Figure 32: Viscosity (Pa*s) vs Shear Rate (1/s) profiles of a) CS, 8DEX, 8PULL, 10DEX, 10PULL and b) CS20DEX8, CS20DEX10, CS20PULL8, CS20PULL10. Data are expressed as mean values ± sd n=3.*

For this reason, the rheological synergism was calculated to investigate the eventual presence of interactions between the polymers composing the MNs-forming solutions. As reported in Figure 33, it was possible to observe an increase in the synergistic effect as the concentration of DEX or PULL increased from 8% to 10%. Furthermore, PULL-based formulations showed a higher rheological synergism compared to DEX-based formulations, probably suggesting a higher degree of interaction between CS and PULL. In detail, CS20PULL10 showed the strongest synergistic effect.

The higher rheological synergism observed for PULL-based formulations may be related to the different molecular structure of PULL compared with DEX. Both polymers are rich in hydroxyl groups and can interact with CS mainly through hydrogen bonding and physical chain entanglement. However, the more linear and flexible structure of PULL may favor closer interactions with CS chains, leading

to a more interconnected polymeric network and, consequently, to a higher viscosity. In contrast, the more branched structure of DEX may limit extensive chain interactions, resulting in a less pronounced synergistic effect [53,69,70]

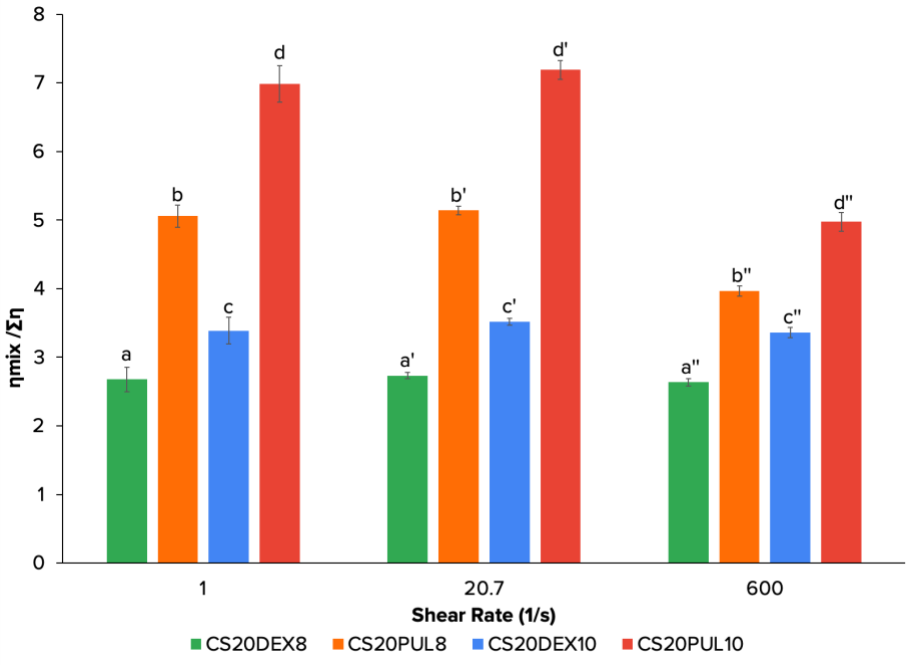

Figure 33: $\eta_{mix}/\sum\eta$ vs at 1 s-1, 20 s-1 and 600 s-1 of CS20DEX8, CS20DEX10, CS20PULL8, CS20PULL10 DMNs. Data are expressed as mean values ± sd, n=3. ANOVA one way post hoc Scheffè test (p value≤0.05): a vs b,c,d; b vs c,d; c vs d; a' vs b', c', d'; b' vs c', d'; c' vs d'; a'' vs b'',c'',d''; b''vs c'', d''; c'' vs d''.

To further investigate the mechanical performance of the selected DMNS, their insertion capability was evaluated using the Parafilm® model, as described in Section 6.2.6. This test was performed to predict the ability of the MNs to penetrate a skin-like membrane and to compare the insertion performance of the different formulations.

The results reported in Figure 34 as number of holes generated for each Parafilm® layer, including its corresponding depth. Moreover, PR% was calculated for all formulations for each Parafilm® layer and reported in Table 2.

As can be appreciated, all DMNs demonstrated that all four formulations were able to perforate the first Parafilm® layer with a PR% of 100% in all cases.

Remarkably, almost all MNs successfully penetrated also the second Parafilm® layer, corresponding to an approximate depth of 400 μm, with a PR% ranging between 99 and 100%. This result suggests that the selected DMNs possessed sufficient mechanical strength to overcome the resistance of the membrane and potentially reach the superficial skin layers.

The DMNs were also able to reach deeper layers, up to the fourth Parafilm® layer, corresponding to approximately 800 μm. However, at this depth, only part of the array produced visible holes, indicating that deeper penetration was not achieved by all needles under the applied force as it can be view in Table 2.

Table 2: Penetration rate % (PR %) of selected DMNs for each Parafilm® layer.

Parafilm layer	CS20DEX8	CS20DEX10	CS20PULL8	CS20PULL10
1	100	100	100	100
2	100	100	99	100
3	71	100	89	46
4	11	27	10	2
5	0	0	0	0
6	0	0	0	0
7	0	0	0	0
8	0	0	0	0

Among the tested formulations, the CS20DEX10 achieved the highest insertion depth, as demonstrated by the greatest number of perforations in the deeper Parafilm® layers. Interestingly, although the PULL-based formulations exhibited higher viscosity and greater rheological synergism, this did not translate into superior insertion performance. This suggests that MNs penetration capacity depends on a combination of factors, including morphology, stiffness, toughness, and polymer composition.

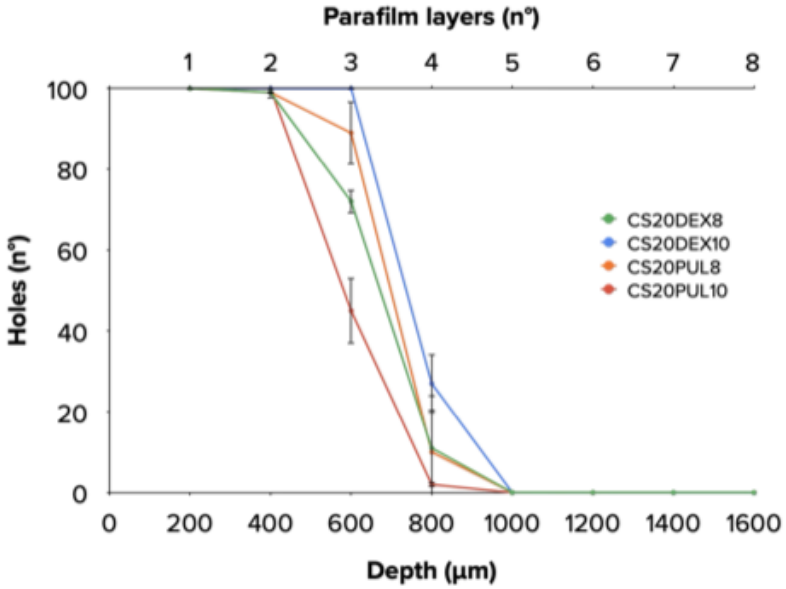

Figure 34: Number (n°) of Holes vs Depth (µm) calculated for CS20DEX8, CS20DEX10, CS20PULL8, CS20PULL10 DMNs. Data are expressed as mean values ± sd, n=3..

Finally, to achieve a complete mechanical characterization of the selected MNs, dynamic mechanical analysis was also performed in compression test, as described in Section 6.2.7.

First, an amplitude sweep test was first carried out in strain-controlled mode to identify the linear viscoelastic region (LVR) of each formulation. As shown in Figure 35, all four formulations exhibited a similar trend with increasing strain, indicating comparable viscoelastic behavior. Based on these results, a strain value

of 0.315%, corresponding to approximately the 2/3 of the LVR for all samples, was selected for the subsequent frequency sweep tests.

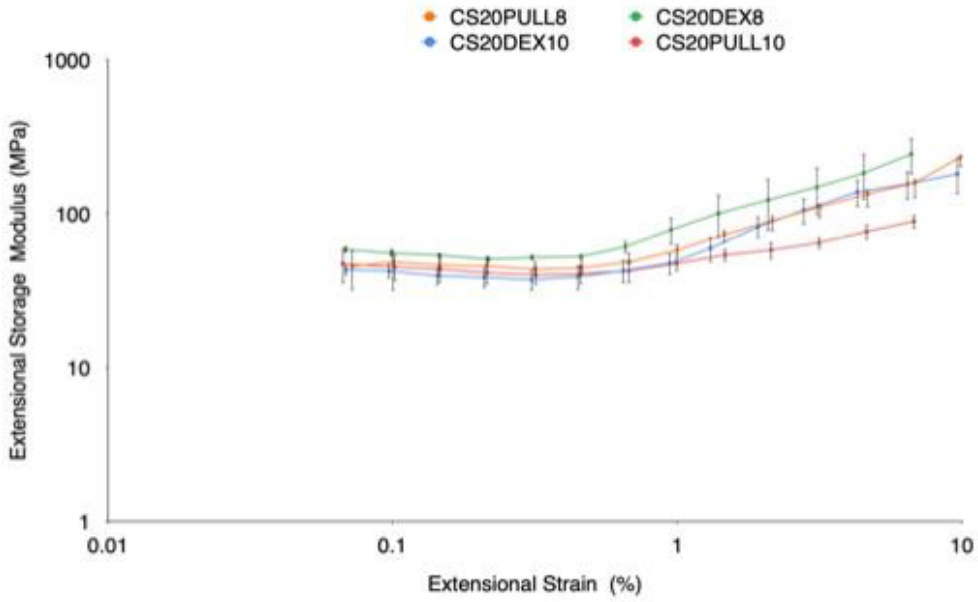

Figure 35: Extensional storage modulus (MPa) of CS20DEX8, CS20DEX10, CS20PULL8, CS20PULL10 DMNs at increasing shear strain % (0.01-10%). Data are expressed as mean values ± sd, n=3.

Following, the frequency sweep test was performed and the results are reported in Figure 36. It can be observed that, for all the formulations, the storage modulus (E′) was significantly higher than the loss modulus (E″) over the entire frequency range. This indicates that the MNs exhibited a predominantly elastic, solid-like behavior. For all formulations, both E' and E'' remained nearly constant over the entire frequency range, indicating a good stability of the DMNs under the investigated conditions.

Only minor differences were observed among the four formulations. Overall, DEX-based MNs showed higher E' moduli when compared to the PULL-containing ones.

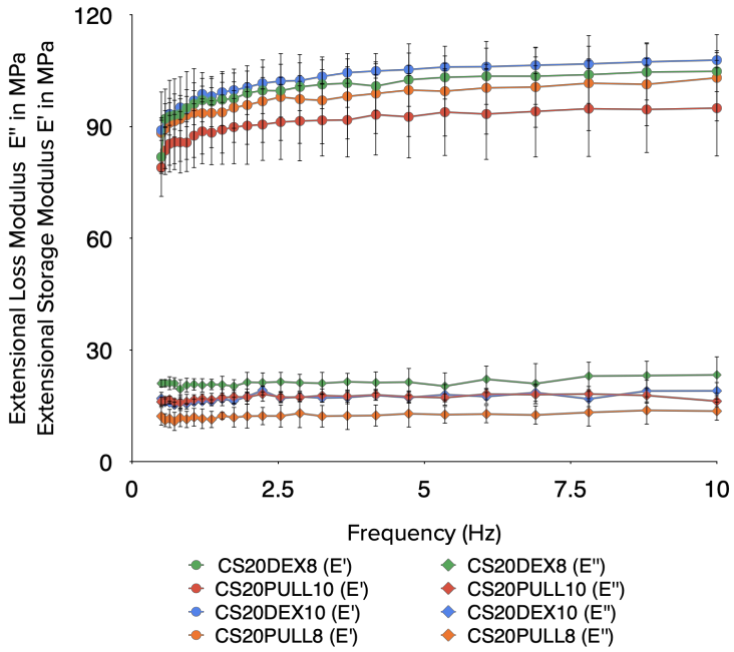

Figure 36: Extensional Loss and Storage Moduli (MPa) of CS20DEX8, CS20DEX10, CS20PULL8, CS20PULL10 DMNs in a 0.5 -10 Hz Frequency (Hz) range. Data are expressed as mean values ± sd, n=3.

The viscoelastic behavior was further investigated by the calculation of the extensional loss factor (tgδ). Tgδ values of the selected MNs, calculated at 2.5 Hz are reported in Figure 37. As expected, all DMNs are characterized by tgδ values lower than 1, typical of solid-like materials. In particular, among the formulations, CS20PUL8 showed the lowest tan δ values, suggesting a more elastic response compared with the other samples.

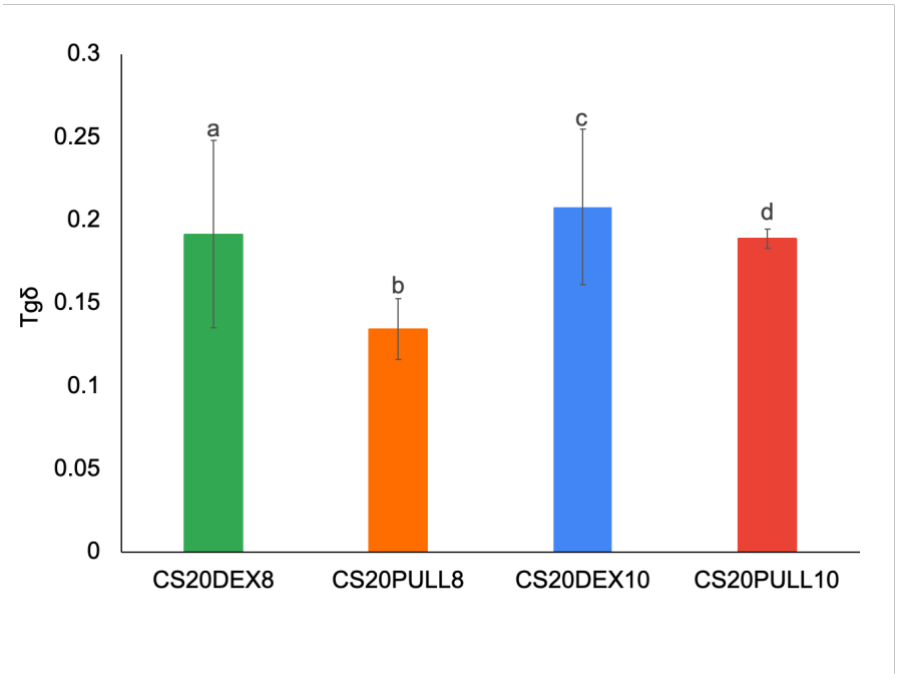

Figure 37: Tg δ values calculated at 2.5 (Hz) of selected DMNs. Data are expressed as mean values ± sd, n=3 ANOVA one way; post hoc Scheffè test (p value ≥0.05): no statistically significant different was observed.

After evaluating the morphological and mechanical properties of the MNs, a dissolving test was performed on an agarose/gelatine (AG/GEL) biomimetic skin mimicking bilayer hydrogel, prepared according to Section 6.2.10, in order to investigate the dissolution behavior of the selected DMNs. In detail, such bilayer hydrogel is characterized by two layers containing two different water contents, in order to simulate the water content of the stratum corneum and epidermis layer, respectively.

To simulate MNs dissolution behavior upon insertion into the skin, the MN arrays were inserted into the hydrogel using the dedicated Microapplicator and maintained in contact with the hydrogel for different time intervals before being removed for morphological evaluation. Results are reported in Figure 38 showing each MN array after MNs removal at each time point.

As can be observed, no appreciable dissolution was observed after either 5 or 10 minutes of insertion for all MNs, as they retained their original geometry and dimensions. Interestingly, after 20 minutes, the needle tips began to show signs of dissolution, resulting in a reduction in needle length. This effect became more evident after 30 minutes, indicating the progressive dissolution of the polymeric matrix within the hydrated milieu of the hydrogel.

Finally, the most pronounced changes were observed after 40 minutes of insertion. At this time point, most of the MNs undergone extensive dissolution, with a substantial reduction in their length.

Both DEX-containing DMNs showed a greater extent of dissolution than the corresponding PULL-containing formulations. This finding may be related to the stronger interactions between PULL and CS previously suggested by the rheological synergism analysis. These interactions could reduce water penetration into the polymeric matrix and slow down the dissolution of CSPULL MNs compared with CSDEX systems.

However, the polymer–polymer interactions were not sufficiently strong to prevent MNs dissolution within the investigated time range, without affecting the dissolving properties of the developed MNs. On the contrary, their presence may be advantageous, as it could moderately delay matrix dissolution and provide a short-term controlled release of the incorporated active compound.

a)

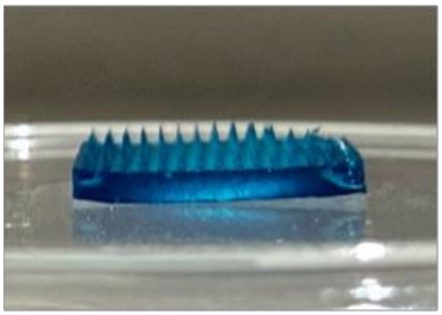

CS20DEX8

b)

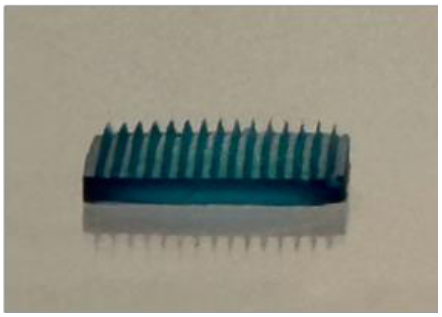

CS20DEX10

c)

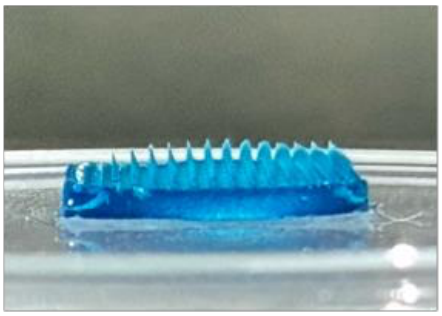

CS20PULL8

d)

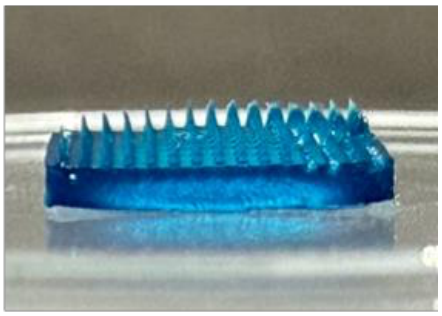

CS20PULL10

After 5 minutes

e)

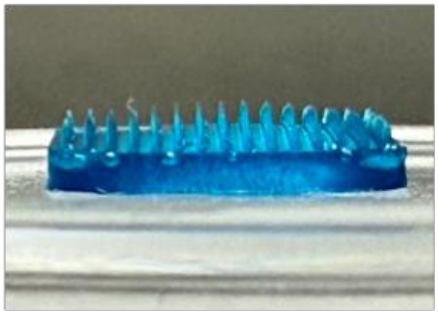

CS20DEX8

f)

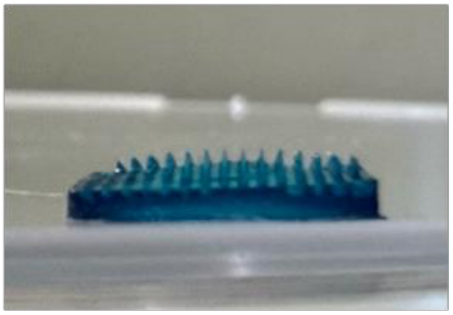

CS20DEX10

g)

CS20PULL8

h)

CS20PULL10

After 10 minutes

i)

CS20DEX8

j)

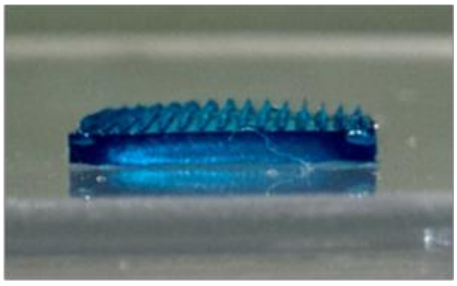

CS20DEX10

k)

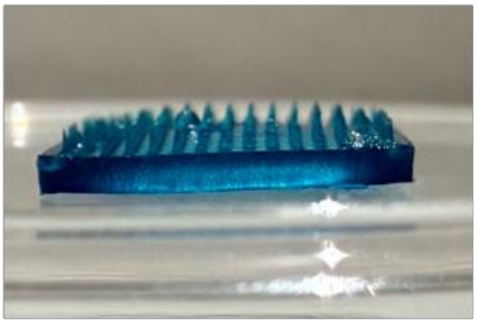

CS20PULL8

l)

CS20PULL10

After 20 minutes

m)

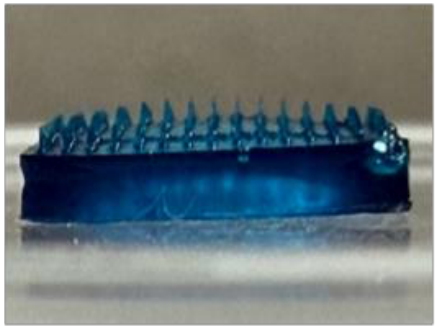

CS20DEX8

n)

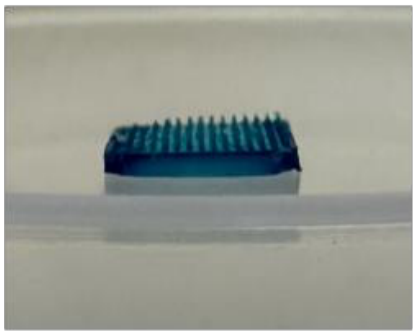

CS20DEX10

o)

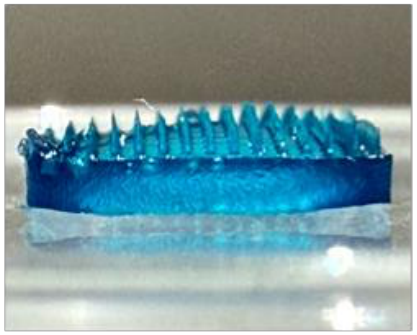

CS20PULL8

After 30 minutes

p)

CS20PULL10

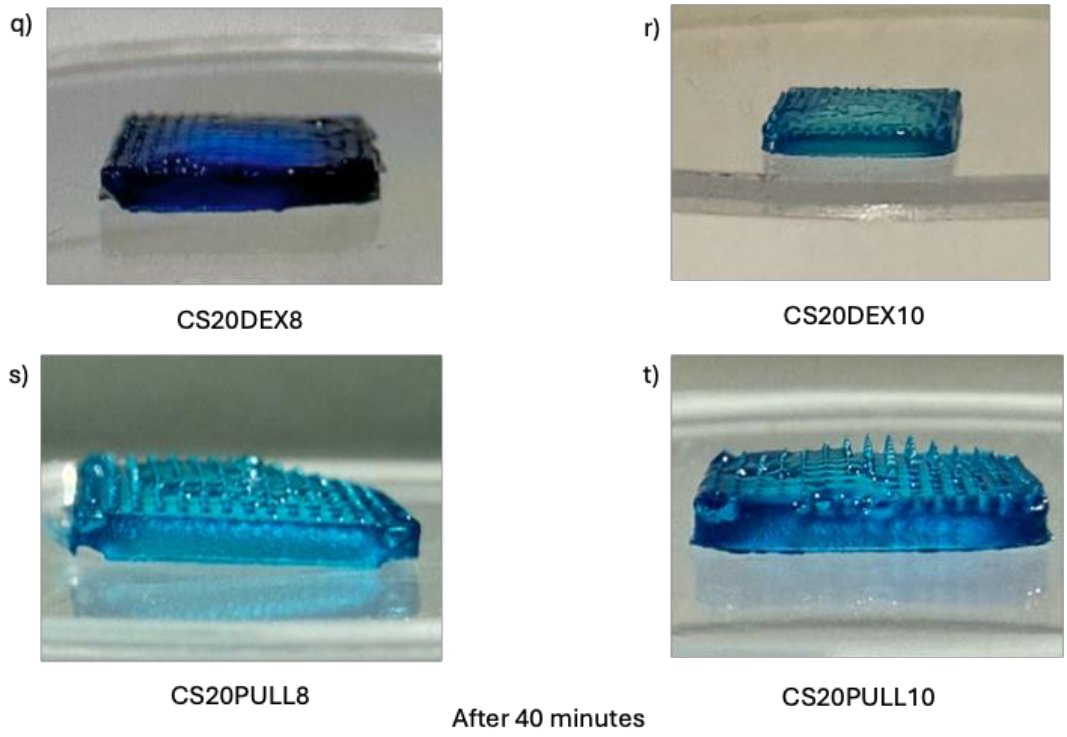

Figure 38: Images of DMNs after removal from the bilayer skin-mimicking hydrogel at 5, 10, 20, 30 and 40 minutes.

In addition, a representative image of the hydrogel after CS20PULL8 removal is reported in Figure 39. From the image it can be appreciated the presence of methylene blue within the matrix, confirming the release of material from the DMNs, providing visual evidence of polymer dissolution. Overall, these results demonstrate the progressive dissolution of the MNs under hydrated conditions, indicating that the selected formulations can maintain sufficient structural integrity for insertion while gradually dissolving after application. This behavior is desirable for DMNs systems, as it enables the release of the incorporated compounds directly into the skin.

Figure 39: Image of hydrogel with methylene blue residues after CS20DEX8 removal.

Afterwards thermal behavior of all MNs was assessed by means of Thermogravimetric analysis (TGA) and Differential Scanning Calorimetry (DSC) analysis. In detail, TGA and Differential Scanning Calorimetry DSC thermograms all the four types of MNs are reported in Figure 40 and Figure 41. Thermal analysis was performed to investigate the residual moisture content and the thermal behavior of the developed MNs.

In all formulations, TGA showed an initial mass loss at relatively low temperatures, which was mainly attributed to the evaporation of residual free and weakly bound water. In the CS/DEX systems, this first weight loss was approximately 7.6% (CS20DEX8) and 4.7% (CS20DEX10), whereas in the CS/PULL systems it was about 8.6% (CS20PULL8) and 5.2%. (CS20PULL10) These results indicate that all formulations retained a certain amount of residual moisture after preparation. In particular MNs with the secondary polymers at 10% demonstrated a lower amount of residual water if compared to the 8%-containing

ones. Moreover, slightly higher values were observed for the PULL-based systems.

At higher temperatures, additional weight losses were detected, which can be ascribed to the thermal degradation of the polysaccharide matrix. Since these later events may include contributions from both strongly bound water and polymer decomposition, they were not considered representative of residual moisture alone. Therefore, the initial low-temperature mass loss was taken as the most reliable indicator of the residual water content.

DSC thermograms supported the TGA findings. All formulations showed a broad endothermic event in the approximate range of 75–100 °C, which can be attributed to the evaporation of water associated with the hydrophilic polymer network. The broad shape of this endotherm suggests that water was present in different states. No sharp melting transitions were observed, in agreement with the predominantly amorphous nature of the polysaccharide-based matrices.

Overall, the combined TGA and DSC results indicate that the DMNs contained residual moisture and that water was not present only as free water, but also as water interacting with the polymer chains. The slightly higher residual water content observed for the CS/PULL systems may reflect a greater water-retention ability of pullulan-containing matrices. This interpretation is coherent with the rheological synergism previously observed, which suggested stronger intermolecular interactions in the PULL-based formulations. Therefore, thermal analysis supports the hypothesis that the different polysaccharide combinations influenced not only the structural organization of the matrix, but also its interaction with water.

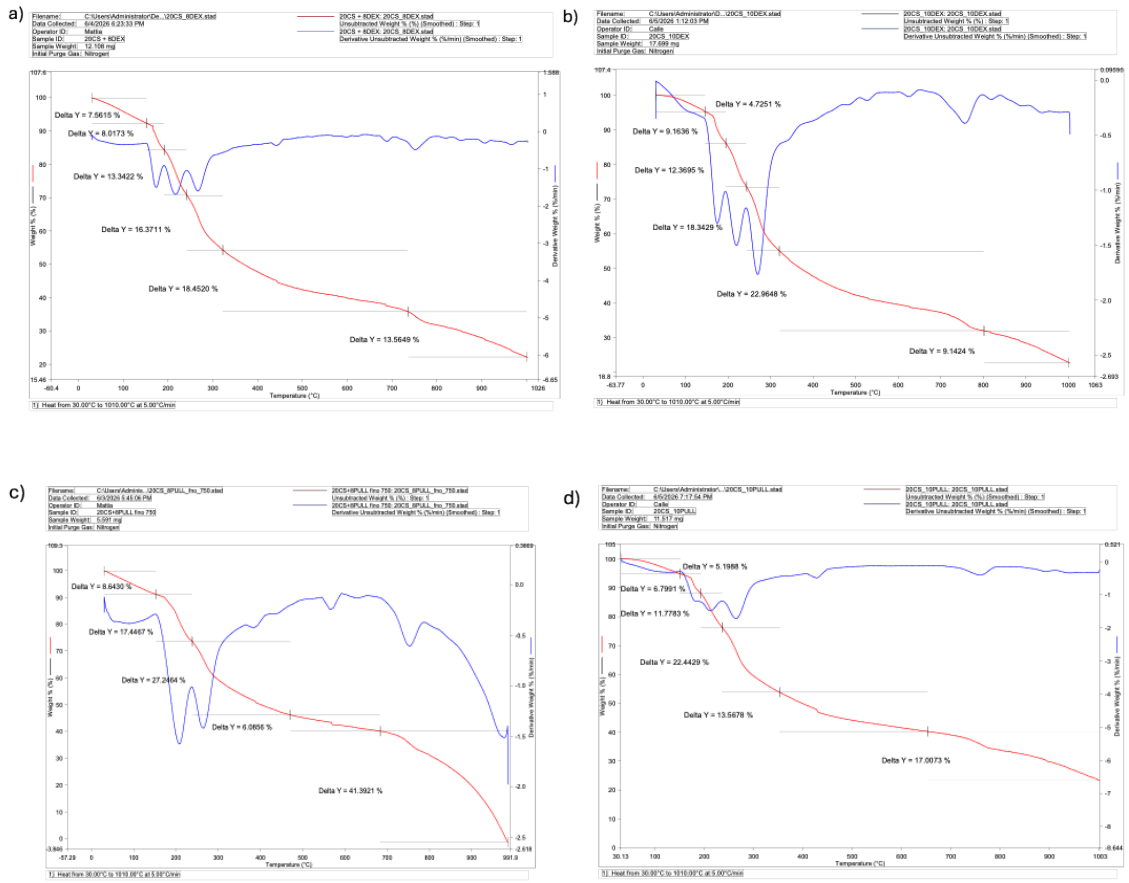

Figure 40: TGA and derivative thermogravimetric (dTGA) curves of DMNs: a) CS20DEX8, b) CS20DEX10, c) CS20PULL8 and d) CS20PULL10 representing the weight % of MNs from 30 up to 1010 °C.

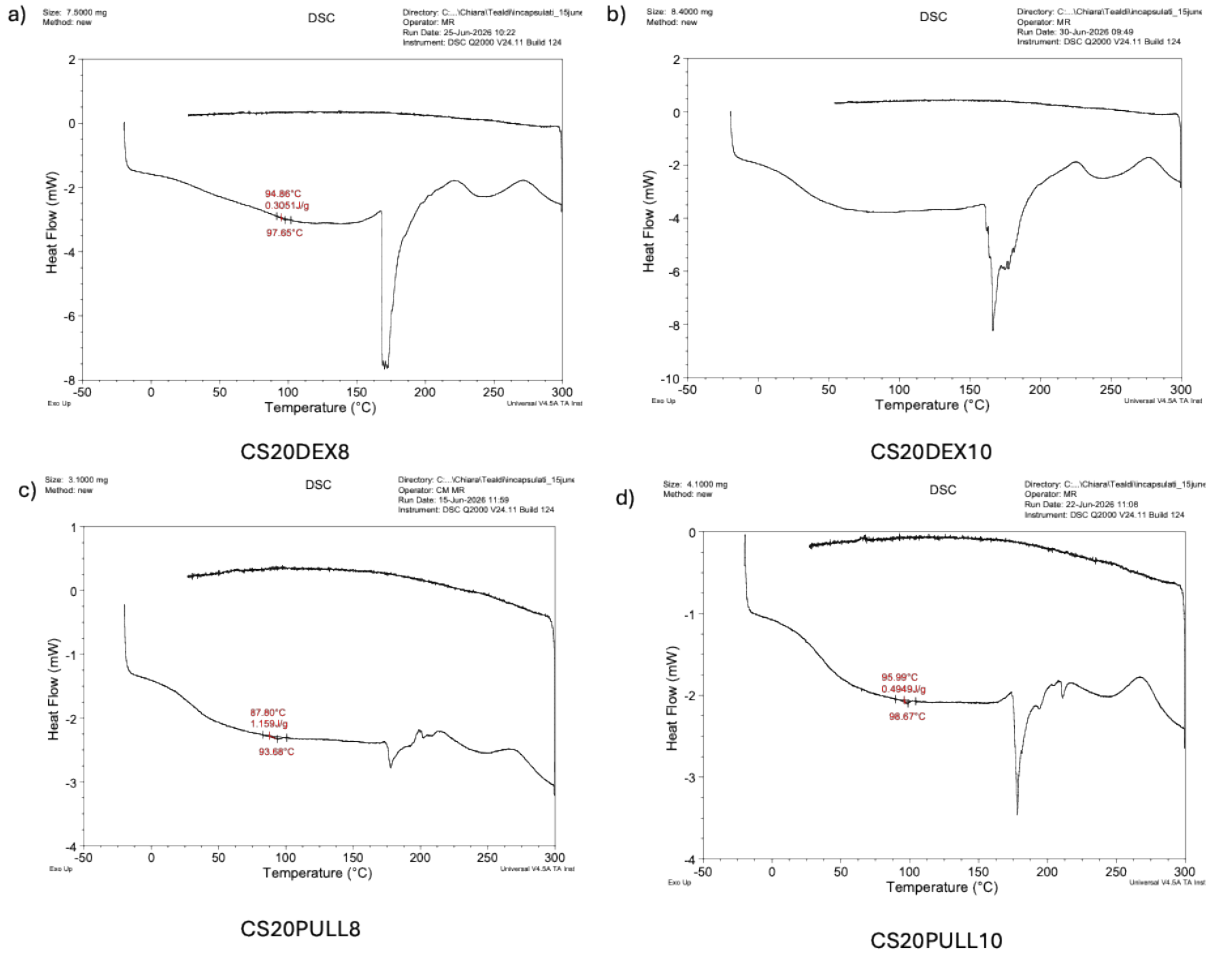

Figure 41: DSC thermograms of CS/DEX and CS/PULL DMNs formulations.

To further investigate the physical-chemical properties of the developed MNs, FT-IR analysis was performed. MNs spectra are reported in Figure 42 a) for DEX-based MNs and b) for PULL-base MNs in comparison with the corresponding physical mixtures (PM).

FT-IR spectra of the MNs and corresponding PM showed the characteristic absorption bands of CS-based polysaccharide systems. In all samples, a broad absorption band was observed around 3300 cm^{-1}, attributable to O–H stretching vibrations, while the band near 2924-2925 cm^{-1} was associated with C–H stretching. Additional bands were detected at

approximately 1604-1606 cm^{-1} and 1407-1409 cm^{-1}, which can be assigned to carboxylate-related vibrations, whereas the absorptions around 1226–1228 cm^{-1} and 1007–1016 cm^{-1} were associated with sulphate and C–O/C–O–C vibrations characteristic of the polysaccharide structure.

No new bands were detected after MNs preparation, indicating that the manufacturing process did not induce evident chemical modifications or the formation of new covalent bonds. However, slight variations in band shape, intensity, and position were observed when comparing the PM with the corresponding MNs, particularly in the O–H stretching region and in the fingerprint region. These changes suggest the occurrence of intermolecular interactions between CS and the second polysaccharide, most likely through hydrogen bonding.

This interpretation is consistent with the rheological synergism analysis, which demonstrated the presence of polymer–polymer interactions in both systems and showed a more pronounced synergistic effect in the PULL-based formulations than in the dextran-based ones. In this context, the FT-IR results support the hypothesis that PULL established stronger interactions with CS than DEX. This behaviour is also in line with the thermal analysis, which indicated slightly greater residual moisture in the CS/PULL systems, further suggesting a different organization of the polymer network and its interaction with water.

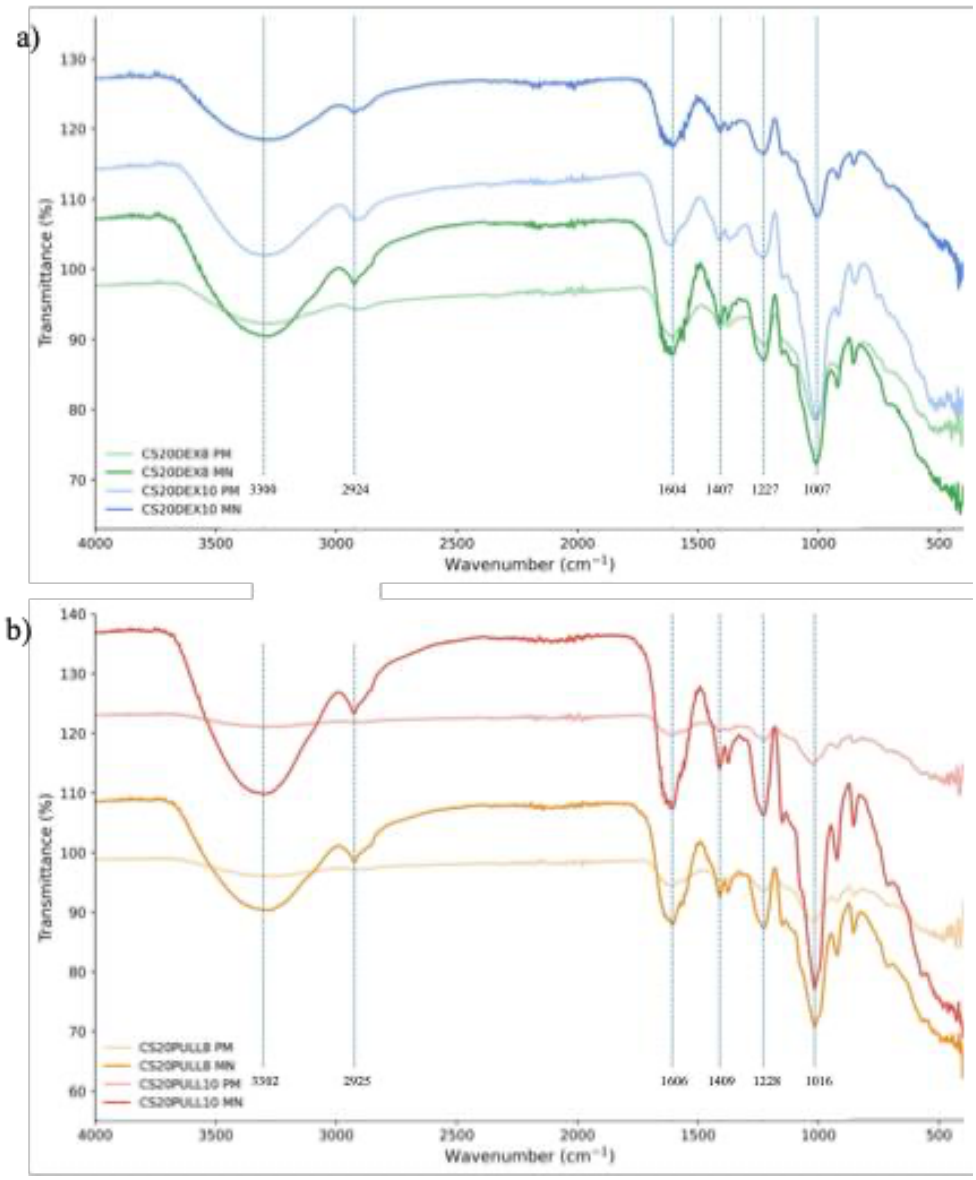

Figure 42: FT-IR spectra of CSDEX and CSPULL MNs in comparison with their corresponding physical mixtures (PM). Spectra are reported as transmittance (%) and were vertically offset for clarity. The main absorption bands are indicated by their corresponding wavenumbers.

Lastly, FITC-albumin was used as protein model to be loaded into the MNs, in order to evaluate the drug-loading properties of the developed MNs. FITC-Albumin was loaded at a concentration of 2 mg/ml, as already reported in literature. From the spectrofluorimetric analysis, a recovery of 37.5% was obtained.

8. CONCLUSION

The present thesis focuses on the development of dissolving microneedles (DMNs) based on chondroitin sulfate (CS) combined with either dextran (DEX) or pullulan (PULL), with the final aim of obtaining an innovative platform suitable for the delivery of protein-based vaccines.

Different polymeric formulations were initially prepared and characterized by rheological analysis to establish the most suitable concentrations of the polymers for the further development of MNs. The polymeric solutions were processed by micromolding assisted by solvent evaporation, and the morphology of the resulting MNs was evaluated by SEM analysis. Although all the formulations investigated allowed the formation of MNs, differences were observed in terms of array homogeneity, tip definition, and structural integrity. Compression testing further confirmed the influence of polymer composition on the behavior of the DMNs. The mechanical characterization results were further confirmed by morphological analysis of MNs after compression by means of SEM.

Based on both morphological and mechanical results, four formulations were selected for further investigation: CS20DEX8, CS20DEX10, CS20PULL8, and CS20PULL10. These formulations showed the most favorable balance between mold filling, needle definition, and mechanical resistance.

In addition, a more detailed rheological investigation revealed a positive synergistic effect between CS and the secondary polymers. This effect was more pronounced for PULL-containing formulations, suggesting stronger physical interactions between CS and PULL than between CS and DEX. This behavior could be related to PULL more linear molecular structure compared to DEX, which could more easily facilitate intermolecular interaction with CS.

The insertion capability of the selected formulations was evaluated using the Parafilm® model. Nearly all DMNs were able to penetrate the second Parafilm® layer, corresponding to an approximate depth of 400 μm, while only part of the arrays reached deeper layers. These results suggest that the selected formulations possess suitable mechanical properties to penetrate the stratum corneum and potentially reach the viable epidermidis or superficial dermal region. Nevertheless, ex vivo or in vivo skin models will be required to confirm their actual performance under more physiologically relevant conditions.

Following, Dynamic Mechanical Analysis showed that the storage modulus remained higher than the loss modulus over the investigated frequency range, indicating a predominantly elastic, solid-like behavior for all selected formulations.

A biomimetic bilayer skin-mimicking hydrogel was successfully developed with the aim of simulating the water content of the different skin layers, namely the stratum corneum and the epidermis. The dissolution test performed showed that the MNs progressively dissolved during time, revealing a complete dissolution upon 40 minutes for all DMNs. DEX-containing DMNs dissolved more rapidly than PULL-containing ones, in agreement with the stronger interactions probably occurring between CS and PULL.

Thermal and spectroscopic analyses further supported these findings. TGA revealed an initial mass loss attributable to residual moisture, with slightly higher values observed for the PULL-containing formulations. DSC showed broad low-temperature endothermic events associated with water evaporation from the hydrophilic polymeric matrices, indicating that water was present in different states of association with the polymer chains. FT-IR spectra results highlighted slight variations in band shape and position, particularly in the O–H stretching and

fingerprint regions, which were consistent with the establishment of intermolecular interactions between CS and the secondary polymers. These changes appeared more evident in the PULL-containing systems and were therefore in agreement with the rheological synergism results.

Finally, FITC-albumin was successfully incorporated into the CS20DEX8 formulation. Spectrofluorimetric analysis showed a recovery of approximately 40%, demonstrating the feasibility of protein loading while also highlighting the need for further optimization.

Overall, the results indicate that CS-based dissolving MNs containing DEX or PULL represent promising candidates for protein delivery.

Future studies should focus on improving protein recovery, confirming protein stability after fabrication, evaluating release kinetics, and assessing insertion using more representative ex vivo and in vivo skin models.

9. BIBLIOGRAPHY

[1] O. Arda, N. Göksügür, Y. Tüzün, Basic histological structure and functions of facial skin, Clin. Dermatol. 32 (2014) 3–13. https://doi.org/10.1016/j.clindermatol.2013.05.021.

[2] FREDERIC H. MARTINI • ROBERT B. TALLITSCH • Judi L.. NATH, HUMAN ANATOMY, VII, EdiSES S.r.l., Napoli, 2019.

[3] Wilfredo Lopez-Ojeda; Amarendra Pandey; Mandy Alhajj; Amanda M. Oakley, Anatomy, skin (integument), StatPearls, 2022.

[4] S. Knox, N.M. O'Boyle, Skin lipids in health and disease: A review, Chem. Phys. Lipids 236 (2021). https://doi.org/10.1016/j.chemphyslip.2021.105055.

[5] G. Kim, H. Ahn, J. Chaj Ulloa, W. Gao, Microneedle sensors for dermal interstitial fluid analysis, Med-X 2 (2024). https://doi.org/10.1007/s44258-024-00028-0.

[6] A. Lefèvre-Utile, C. Braun, M. Haftek, F. Aubin, Five functional aspects of the epidermal barrier, Int. J. Mol. Sci. 22 (2021). https://doi.org/10.3390/ijms222111676.

[7] Sanjay Agarwal; Karthik Krishnamurthy, Histology, skin , StatPearls, 2023.

[8] C. Prost-Squarcioni, S. Fraitag, M. Heller, N. Boehm, Functional histology of dermis, Ann. Dermatol. Venereol. 135 (2008) 5–20. https://doi.org/10.1016/s0151-9638(08)70206-0.

[9] G.m.pontieri-PatologiaGeneralePerICorsiDiLaureaInProfessioniSanitarie-Piccin, (n.d.).

[10] C.T. Berry, C.S. Frazee, P.J. Herman, S. Chen, A. Chen, Y. Kuo, C.T. Ellebrecht, Current advancements in cellular immunotherapy for autoimmune disease, Semin. Immunopathol. 47 (2025). https://doi.org/10.1007/s00281-024-01034-5.

[11] D. Liu, T. Zhao, Y. Li, L. Huang, J. Che, P. Zou, W. Yang, J. Ding, P. Wu, X. Gao, Y. Ran, H. Sun, Z. Li, J. Gao, C. Gao, Nanocarrier-based immunotherapy for viral diseases, Int. J. Pharm. X 10 (2025). https://doi.org/10.1016/j.ijpx.2025.100408.

[12] R. Rappuoli, Vaccines: Science, health, longevity, and wealth, Proc. Natl. Acad. Sci. U. S. A. 111 (2014) 12282. https://doi.org/10.1073/pnas.1413559111.

[13] A.M. Stern, H. Markel, The history of vaccines and immunization: Familiar patterns, new challenges - If we could match the enormous scientific strides of the twentieth century with the political and economic investments of the nineteenth, the world's citizens might be much healthier, Health Aff. 24 (2005) 611–621. https://doi.org/10.1377/hlthaff.24.3.611.

[14] I. Menon, P. Bagwe, K.B. Gomes, L. Bajaj, R. Gala, M.N. Uddin, M.J. D'souza, S.M. Zughaier, Microneedles: A new generation vaccine delivery system, Micromachines (Basel). 12 (2021). https://doi.org/10.3390/mi12040435.

[15] S.A. Shah, R.S. Oakes, S.M. Kapnick, C.M. Jewell, Mapping the Mechanical and Immunological Profiles of Polymeric Microneedles to Enable Vaccine and Immunotherapy Applications, Front. Immunol. 13 (2022). https://doi.org/10.3389/fimmu.2022.843355.

[16] L. Zhang, W. Wang, S. Wang, Effect of vaccine administration modality on immunogenicity and efficacy, Expert Rev. Vaccines 14 (2015) 1509–1523. https://doi.org/10.1586/14760584.2015.1081067.
[17] I. Menon, P. Bagwe, K.B. Gomes, L. Bajaj, R. Gala, M.N. Uddin, M.J. D'souza, S.M. Zughaier, Microneedles: A new generation vaccine delivery system, Micromachines (Basel). 12 (2021). https://doi.org/10.3390/mi12040435.
[18] G.N. Yıldız, D. Koçyiğit, G. Koç, B. Yavuz, H.D. Yüce Başaran, B. Çiftçi, Factors Affecting Pain, Fear, and Comfort Levels After Intramuscular Injection and Nursing Strategies, Pain Management Nursing (2026). https://doi.org/10.1016/j.pmn.2026.03.003.
[19] Y.C. Kim, C. Jarrahian, D. Zehrung, S. Mitragotri, M.R. Prausnitz, Delivery systems for intradermal vaccination, Curr. Top. Microbiol. Immunol. 351 (2012) 77–112. https://doi.org/10.1007/82_2011_123.
[20] F.K. Aldawood, A. Andar, S. Desai, A comprehensive review of microneedles: Types, materials, processes, characterizations and applications, Polymers (Basel). 13 (2021). https://doi.org/10.3390/polym13162815.
[21] A. Tucak, M. Sirbubalo, L. Hindija, O. Rahić, J. Hadžiabdić, K. Muhamedagić, A. Čekić, E. Vranić, Microneedles: Characteristics, materials, production methods and commercial development, Micromachines (Basel). 11 (2020). https://doi.org/10.3390/mi11110961.
[22] A.Z. Alkilani, M.T.C. McCrudden, R.F. Donnelly, Transdermal drug delivery: Innovative pharmaceutical developments based on disruption of the barrier properties of the stratum corneum, Pharmaceutics 7 (2015) 438–470. https://doi.org/10.3390/pharmaceutics7040438.
[23] Y.C. Kim, J.H. Park, M.R. Prausnitz, Microneedles for drug and vaccine delivery, Adv. Drug Deliv. Rev. 64 (2012) 1547–1568. https://doi.org/10.1016/j.addr.2012.04.005.
[24] N. Joshi, S. Azizi Machekposhti, R.J. Narayan, Evolution of Transdermal Drug Delivery Devices and Novel Microneedle Technologies: A Historical Perspective and Review, JID Innov. 3 (2023). https://doi.org/10.1016/j.xjidi.2023.100225.
[25] M.I. Haq, E. Smith, D.N. John, M. Kalavala, C. Edwards, A. Anstey, A. Morrissey, J.C. Birchall, Clinical administration of microneedles: Skin puncture, pain and sensation, Biomed. Microdevices 11 (2009) 35–47. https://doi.org/10.1007/s10544-008-9208-1.
[26] R.F. Maia, P. Machado, R.O. Rodrigues, V. Faustino, H. Schütte, S. Gassmann, R.A. Lima, G. Minas, Recent advances and perspectives of MicroNeedles for biomedical applications, Biophys. Rev. 17 (2025) 909–928. https://doi.org/10.1007/s12551-025-01317-7.
[27] A.H. Sabri, J. Ogilvie, K. Abdulhamid, V. Shpadaruk, J. McKenna, J. Segal, D.J. Scurr, M. Marlow, Expanding the applications of microneedles in dermatology, European Journal of Pharmaceutics and Biopharmaceutics 140 (2019) 121–140. https://doi.org/10.1016/j.ejpb.2019.05.001.
[28] M. Zheng, T. Sheng, J. Yu, Z. Gu, C. Xu, Microneedle biomedical devices, Nature Reviews Bioengineering 2 (2024) 324–342. https://doi.org/10.1038/s44222-023-00141-6.

[29] B. Jia, T. Xia, X. Wang, Y. Xu, Z. Guo, Morphology design of polymer microneedle arrays: Key factors from the application perspective, J. Drug Deliv. Sci. Technol. 88 (2023). https://doi.org/10.1016/j.jddst.2023.104883.
[30] C. Pereira-Leite, A. Júlio, M. Visscher, H.W. Frijlink, W.L.J. Hinrichs, What Is the Optimal Geometry of Dissolving Microneedle Arrays? A Literature Review, Pharmaceutics 17 (2025) 124. https://doi.org/10.3390/pharmaceutics.
[31] I. Mansoor, H.A. Eassa, K.H.A. Mohammed, M.A. Abd El-Fattah, M.H. Abdo, E. Rashad, H.A. Eassa, A. Saleh, O.M. Amin, M.I. Nounou, O. Ghoneim, Microneedle-Based Vaccine Delivery: Review of an Emerging Technology, AAPS PharmSciTech 23 (2022). https://doi.org/10.1208/s12249-022-02250-8.
[32] O. Olatunji, D.B. Das, M.J. Garland, L. Belaid, R.F. Donnelly, Influence of array interspacing on the force required for successful microneedle skin penetration: Theoretical and practical approaches, J. Pharm. Sci. 102 (2013) 1209–1221. https://doi.org/10.1002/jps.23439.
[33] J.H. Jung, S.G. Jin, Microneedle for transdermal drug delivery: current trends and fabrication, J. Pharm. Investig. 51 (2021) 503–517. https://doi.org/10.1007/s40005-021-00512-4.
[34] Z. Sartawi, C. Blackshields, W. Faisal, Dissolving microneedles: Applications and growing therapeutic potential, Journal of Controlled Release 348 (2022) 186–205. https://doi.org/10.1016/j.jconrel.2022.05.045.
[35] R. Nagarkar, M. Singh, H.X. Nguyen, S. Jonnalagadda, A review of recent advances in microneedle technology for transdermal drug delivery, J. Drug Deliv. Sci. Technol. 59 (2020). https://doi.org/10.1016/j.jddst.2020.101923.
[36] R.S.J. Ingrole, H.S. Gill, Microneedle coating methods: A review with a perspective, Journal of Pharmacology and Experimental Therapeutics 370 (2019) 555–569. https://doi.org/10.1124/jpet.119.258707.
[37] Y. Liu, T. Huang, Z. Qian, W. Chen, Extensible and swellable hydrogel-forming microneedles for deep point-of-care sampling and drug deployment, Chinese Chemical Letters 34 (2023). https://doi.org/10.1016/j.cclet.2022.108103.
[38] B. Shriky, M. Babenko, B.R. Whiteside, Dissolving and Swelling Hydrogel-Based Microneedles: An Overview of Their Materials, Fabrication, Characterization Methods, and Challenges, Gels 9 (2023). https://doi.org/10.3390/gels9100806.
[39] Y. Zhang, H. Li, G. Li, Y. Chen, Y. Zeng, Hydrogel-forming microneedles for the treatment of skin diseases, Mater. Today Bio 35 (2025). https://doi.org/10.1016/j.mtbio.2025.102448.
[40] R. Liu, A. Li, Y. Lang, H. Cai, X. Tang, D. Li, X. Liu, J. Liu, Stimuli-responsive polymer microneedles: A rising transdermal drug delivery system and Its applications in biomedical, J. Drug Deliv. Sci. Technol. 88 (2023). https://doi.org/10.1016/j.jddst.2023.104922.
[41] P. Makvandi, R. Jamaledin, G. Chen, Z. Baghbantaraghdari, E.N. Zare, C. Di Natale, V. Onesto, R. Vecchione, J. Lee, F.R. Tay, P. Netti, V. Mattoli, A. Jaklenec, Z. Gu, R. Langer, Stimuli-responsive transdermal microneedle patches, Materials Today 47 (2021) 206–222. https://doi.org/10.1016/j.mattod.2021.03.012.

[42] F.K. Aldawood, A. Andar, S. Desai, Investigating Laser Ablation Process Parameters for the Fabrication of Customized Microneedle Arrays for Therapeutic Applications, Pharmaceutics 16 (2024). https://doi.org/10.3390/pharmaceutics16070885.
[43] B. Liu, X. Yi, Y. Zheng, Z. Yuan, J. Yang, J. Yang, X. Yu, L. Jiang, C. Wang, A Review of Nano/Micro/Milli Needles Fabrications for Biomedical Engineering, Chinese Journal of Mechanical Engineering (English Edition) 35 (2022). https://doi.org/10.1186/s10033-022-00773-6.
[44] J.M. Loh, Y.J.L. Lim, J.T. Tay, H.M. Cheng, H.L. Tey, K. Liang, Design and fabrication of customizable microneedles enabled by 3D printing for biomedical applications, Bioact. Mater. 32 (2024) 222–241. https://doi.org/10.1016/j.bioactmat.2023.09.022.
[45] K. Ita, Ceramic microneedles and hollow microneedles for transdermal drug delivery: Two decades of research, J. Drug Deliv. Sci. Technol. 44 (2018) 314–322. https://doi.org/10.1016/j.jddst.2018.01.004.
[46] Z. Yuan, H. Zhang, W. Hu, X. Yu, S. Qin, C. Wang, F. Zhang, State-of-the-art Review of Metallic Microneedles: Structure, Fabrication, and Application, Chinese Journal of Mechanical Engineering (English Edition) 38 (2025). https://doi.org/10.1186/s10033-025-01188-9.
[47] N. Sargioti, T.J. Levingstone, E.D. O'Cearbhaill, H.O. McCarthy, N.J. Dunne, Metallic Microneedles for Transdermal Drug Delivery: Applications, Fabrication Techniques and the Effect of Geometrical Characteristics, Bioengineering 10 (2023). https://doi.org/10.3390/bioengineering10010024.
[48] L. Bao, J. Park, G. Bonfante, B. Kim, Recent advances in porous microneedles: materials, fabrication, and transdermal applications, Drug Deliv. Transl. Res. 12 (2022) 395–414. https://doi.org/10.1007/s13346-021-01045-x.
[49] E.M. Eltayib, Fabrication of porous polymeric microneedles: a concise overview, RSC Adv. 15 (2025) 18697–18714. https://doi.org/10.1039/d5ra03274a.
[50] R. Sharma, K. Kuche, P. Thakor, V. Bhavana, S. Srivastava, N.K. Mehra, S. Jain, Chondroitin Sulfate: Emerging biomaterial for biopharmaceutical purpose and tissue engineering, Carbohydr. Polym. 286 (2022). https://doi.org/10.1016/j.carbpol.2022.119305.
[51] S. Mishra, M. Ganguli, Functions of, and replenishment strategies for, chondroitin sulfate in the human body, Drug Discov. Today 26 (2021) 1185–1199. https://doi.org/10.1016/j.drudis.2021.01.029.
[52] P. Du Souich, A.G. García, J. Vergés, E. Montell, Immunomodulatory and anti-inflammatory effects of chondroitin sulphate, J. Cell. Mol. Med. 13 (2009) 1451–1463. https://doi.org/10.1111/j.1582-4934.2009.00826.x.
[53] G. Sun, J.J. Mao, Engineering dextran-based scaffolds for drug delivery and tissue repair, Nanomedicine 7 (2012) 1771–1784. https://doi.org/10.2217/nnm.12.149.
[54] A. Luanda, V. Badalamoole, Past, present and future of biomedical applications of dextran-based hydrogels: A review, Int. J. Biol. Macromol. 228 (2023) 794–807. https://doi.org/10.1016/j.ijbiomac.2022.12.129.
[55] Y. Zhao, S. Jalili, Dextran, as a biological macromolecule for the development of bioactive wound dressing materials: A review of recent progress and future

perspectives, Int. J. Biol. Macromol. 207 (2022) 666–682. https://doi.org/10.1016/j.ijbiomac.2022.02.114.
[56] E. Díaz-Montes, Dextran: Sources, Structures, and Properties, Polysaccharides 2 (2021) 554–565. https://doi.org/10.3390/polysaccharides2030033.
[57] N. Aquinas, C.H. Chithra, M.R. Bhat, Progress in bioproduction, characterization and applications of pullulan: a review, Polymer Bulletin 81 (2024) 12347–12382. https://doi.org/10.1007/s00289-024-05300-2.
[58] R.S. Singh, G.K. Saini, J.F. Kennedy, Pullulan: Microbial sources, production and applications, Carbohydr. Polym. 73 (2008) 515–531. https://doi.org/10.1016/j.carbpol.2008.01.003.
[59] C.K. de Souza, T. Ghosh, N. Lukhmana, S. Tahiliani, R. Priyadarshi, T.G. Hoffmann, S.D. Purohit, S.S. Han, Pullulan as a sustainable biopolymer for versatile applications: A review, Mater. Today Commun. 36 (2023). https://doi.org/10.1016/j.mtcomm.2023.106477.
[60] D.F.S. Fonseca, P.C. Costa, I.F. Almeida, P. Dias-Pereira, I. Correia-Sá, V. Bastos, H. Oliveira, M. Duarte-Araújo, M. Morato, C. Vilela, A.J.D. Silvestre, C.S.R. Freire, Pullulan microneedle patches for the efficient transdermal administration of insulin envisioning diabetes treatment, Carbohydr. Polym. 241 (2020). https://doi.org/10.1016/j.carbpol.2020.116314.
[61] Y.J. Chen, H.W. Cheng, W.Y. Yen, J.H. Tsai, C.Y. Yeh, C.J. Chen, J.T. Liu, S.Y. Chen, S.J. Chang, The Treatment of Keloid Scars via Modulating Heterogeneous Gelatin-Structured Composite Microneedles to Control Transdermal Dual-Drug Release, Polymers (Basel). 14 (2022). https://doi.org/10.3390/polym14204436.
[62] E. Larrañeta, J. Moore, E.M. Vicente-Pérez, P. González-Vázquez, R. Lutton, A.D. Woolfson, R.F. Donnelly, A proposed model membrane and test method for microneedle insertion studies, Int. J. Pharm. 472 (2014) 65–73. https://doi.org/10.1016/j.ijpharm.2014.05.042.
[63] S. Andree, H. Wilms, J. Helfmann, Feasibility of dermal water content determination by spatially resolved reflectance, Medical Laser Application 26 (2011) 109–118. https://doi.org/10.1016/j.mla.2011.05.003.
[64] E.L. Zoudani, P. De Saram, K. Engel, N.T. Nguyen, N. Kashaninejad, Microneedle–Tissue Interaction Across Varying Biological and Mechanical Conditions, Biosensors (Basel). 15 (2025). https://doi.org/10.3390/bios15080521.
[65] W.Y. Seow, K. Kandasamy, G.S.L. Peh, J.S. Mehta, W. Sun, Ultrathin, Strong, and Cell-Adhesive Agarose-Based Membranes Engineered as Substrates for Corneal Endothelial Cells, ACS Biomater. Sci. Eng. 5 (2019) 4067–4076. https://doi.org/10.1021/acsbiomaterials.9b00610.
[66] J.W. Fluhr, R. Darlenski, C. Surber, Glycerol and the skin: Holistic approach to its origin and functions, British Journal of Dermatology 159 (2008) 23–34. https://doi.org/10.1111/j.1365-2133.2008.08643.x.
[67] M.G. McGrath, S. Vucen, A. Vrdoljak, A. Kelly, C. O'Mahony, A.M. Crean, A. Moore, Production of dissolvable microneedles using an atomised spray process: Effect of microneedle composition on skin penetration, European Journal of Pharmaceutics and Biopharmaceutics 86 (2014) 200–211. https://doi.org/10.1016/j.ejpb.2013.04.023.

[68] A.C.Q. Silva, B. Pereira, N.S. Lameirinhas, P.C. Costa, I.F. Almeida, P. Dias-Pereira, I. Correia-Sá, H. Oliveira, A.J.D. Silvestre, C. Vilela, C.S.R. Freire, Dissolvable Carboxymethylcellulose Microneedles for Noninvasive and Rapid Administration of Diclofenac Sodium, Macromol. Biosci. 23 (2023). https://doi.org/10.1002/mabi.202200323.
[69] A. Yemenicioğlu, S. Farris, M. Turkyilmaz, S. Gulec, A review of current and future food applications of natural hydrocolloids, Int. J. Food Sci. Technol. 55 (2020) 1389–1406. https://doi.org/10.1111/ijfs.14363.
[70] S. Tabasum, A. Noreen, M.F. Maqsood, H. Umar, N. Akram, Z. i. H. Nazli, S.A.S. Chatha, K.M. Zia, A review on versatile applications of blends and composites of pullulan with natural and synthetic polymers, Int. J. Biol. Macromol. 120 (2018) 603–632. https://doi.org/10.1016/j.ijbiomac.2018.07.154.